THE ASTROPHYSICAL JOURNAL, 326:19–49, 1988 March 1

SPECTROSCOPY AND PHOTOMETRY OF ELLIPTICAL GALAXIES. V. GALAXY STREAMING TOWARD THE NEW SUPERGALACTIC CENTER[1]

D. LYNDEN-BELL
Institute of Astronomy, The Observatories, Cambridge

S. M. FABER
Lick Observatory, University of California at Santa Cruz

DAVID BURSTEIN
Department of Physics, Arizona State University

ROGER L. DAVIES
Kitt Peak National Observatory, National Optical Astronomy Observatories

ALAN DRESSLER
Mount Wilson and Las Campanas Observatories of the Carnegie Institution of Washington

R. J. TERLEVICH
Royal Greenwich Observatory

AND

GARY WEGNER
Department of Physics and Astronomy, Dartmouth College
Received 1987 April 14; accepted 1987 August 19

ABSTRACT

We analyze here the dynamics of 400 elliptical galaxies of our all-sky survey.

The motions of the elliptical galaxies, over and above Hubble expansion in the Cosmic Microwave Background (CMB) frame, are best fitted by a flow toward a great attractor centered on $l = 307$, $b = 9$ at a distance of $R_m = 4350 \pm 350$ km s^{-1} in the Hubble flow. The excess mass must be $\sim 5.4 \times 10^{16}\ M_\odot$, comparable to the largest superclusters in order to generate the streaming motion at the Sun of 570 ± 60 km s^{-1}. This model, which is an enlarged version of that considered earlier by Shaya, Tammann, and Sandage, and Lilje, Yahil, and Jones, gives a much better fit to the motions of the ellipticals than the bulk motion considered earlier. The latter was itself a much better fit than pure Hubble flow in the CMB frame.

A picture of the hemisphere of sky centered on this direction shows a remarkable concentration of galaxies that broadens the supergalactic band near there (see Fig. 8 in main text). Estimates show that this concentration in Centaurus is some 20 times more populous than the Virgo cluster, although the southern part of the concentration may be obscured by dust in the Milky Way. The Centaurus concentration is behind the big clusters of ellipticals in Centaurus which show large peculiar motions toward it.

The Centaurus concentration both gives more light here and generates more "infall" velocity here than the Virgo cluster, although the latter is at one-third the distance. Because the Centaurus concentration evidently dominates the supergalactic band of galaxies, we suggest that it be called the supergalactic center.

Da Costa *et al.* have published a redshift survey in the direction of the concentration. It shows a strong peak in galaxies with mean heliocentric redshift of 4355 ± 124 km s^{-1} and with a velocity dispersion of 1052 km s^{-1}; transforming to the CMB frame here, the mean velocity is 4654 ± 124 km s^{-1}, in surprisingly good agreement with our totally independent estimate from the motions of ellipticals all around the sky. In the far field, away from Centaurus, we find a negligible streaming, in agreement with the earlier result of Aaronson *et al.*

The value of Ω_0 from these observations is still indeterminate, though higher values near unity are somewhat more compatible than low values. A structure as large as the supercluster could cause a measurable $\Delta T/T$ in the microwave background on scales of 0°.1–1°, especially if Ω_0 is as low as 0.2. Comparison of the observed flow velocities with the cold dark matter model suggests that cold dark matter with biasing parameter $b = 1$ is marginally consistent with the motions, but that $b \geq 2$ is not.

Subject headings: cosmic background radiation — cosmology — galaxies: clustering — galaxies: photometry — galaxies: redshifts

I. INTRODUCTION

a) This Survey

Our survey of all elliptical galaxies with $B < 13.0$ was undertaken to give a large homogeneous body of data on their internal properties. In this way the reality of the correlation found earlier in 24 ellipticals (Terlevich *et al.* 1981) could be unambiguously tested. By deeper studies of cluster ellipticals in Coma, Perseus, Abell 1699, and DC 2345−28 we also hoped to find a more accurate distance indicator than that given by the Faber-Jackson relationship ($L \sim \sigma^x$) between luminosity L and central velocity dispersion σ. Our studies show that σ is

[1] The authors respectfully dedicate this paper to the memory of Marc Aaronson.

well correlated with a precisely defined angular diameter called D_n. In fact, $\sigma^{1.2}/D_n$ is approximately constant for the ellipticals in any one cluster and, since it is proportional to the distance, it provides a very useful distance indicator. It has a factor 2 less scatter than the Faber-Jackson distance indicator $\sigma^{1.75}/L^{1/2}$. The precise definition of D_n is given in § II. A calibration of the new distance indicator using cluster data was described in Dressler *et al.* (1987*b*), and a new calibration is given here. The more accurate distances to elliptical galaxies so found allow us to study deviations from the idealized smooth Hubble expansion. For related studies we see Lucey (1986) and Djorgovski and Davis (1987).

We are led to conclude that the velocity out to 8000 km s^{-1} is not an ideal Hubble flow with respect to the velocity zero point defined by the cosmic microwave radiation. Rather, the flow of elliptical galaxies shows a systematic distortion around the sky, much of which can be accounted for by a 521 km s^{-1} shift of the zero point. In Dressler *et al.* (1987*a*) we reported 599 km s^{-1} for the smaller region $v < 6000$ km s^{-1}. An even better model is obtained with inflow to a concentration of galaxies beyond the centaurus cluster. A great attractor at $l = 307$, $b = 9$ and at a distance corresponding to 4350 km s^{-1} and with sufficient gravity to give an inflow of 570 km s^{-1} at the Local Group provides the best fit to our data.

Details of the systematic choice of our sample of elliptical galaxies, the allocation of their group membership, and tables giving the final values for the basic data are given in Faber *et al.* (1988). These data form the basis for this analysis of the Hubble flow within the volume out to 8000 km s^{-1}. The spectroscopic data are presented in Davies *et al.* (1987), which also gives our assignment of galaxies to groups. A complete listing of all the aperture photometry, much of which was newly determined by us, is given in Burstein *et al.* (1987). Preliminary discussions are in Burstein *et al.* (1986), Faber *et al.* (1987), Lynden-Bell (1986, 1987).

Our galaxy groups were initially found within our data, but most were then identified with those of Huchra and Geller (1982) or Geller and Huchra (1983). Twenty-five groups have two elliptical distances, 31 have three or more, but only five have more than six.

b) Comparison with Other Recent Studies

For studies of the nearby Hubble flow, our data set on elliptical galaxies has the advantages that it contains a large number of objects and covers the whole sky. Figure 1 shows the distribution of the measured galaxies in Galactic coordinates and demonstrates that there is good sky coverage even in the south.

We adopt an analysis scheme that does not require a detailed understanding of the statistical properties of the sample. Further discussion of the selection of the sample and its statistical properties will be given by Faber *et al.* (1988).

The use of elliptical galaxies as opposed to spirals to trace the Hubble flow carries with it some special features. Groups and clusters, to which more accurate distances are determined by taking medians, are common among the ellipticals, and

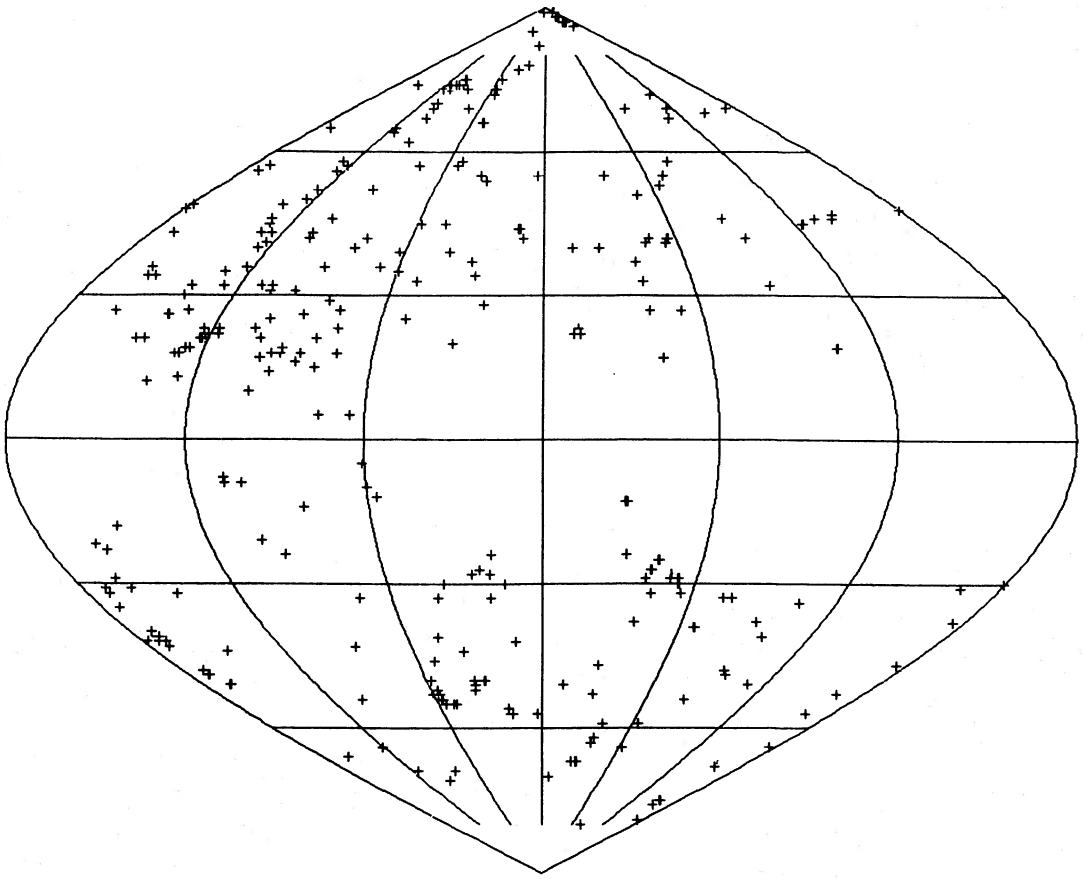

FIG. 1.—The sky distribution of our sample of 385 elliptical galaxies in Galactic coordinates centered as in Fig. 9

group membership is less ambiguous since the ellipticals congregate together more strongly than spirals. Since the cores of ellipticals are reasonably bright, accurate velocity dispersions can be obtained optically for galaxies at redshifts even beyond 10,000 km s^{-1}. This contrasts with the Tully-Fisher method with spirals, for which the very large collecting area of the Arecibo telescope is necessary to determine the 21 cm velocity widths at the higher redshifts. This carries the penalty of the very limited sky coverage of Arecibo unless optical spectra are used.

On the other hand, elliptical galaxies are significantly rarer than spirals, so for studies of the Virgo infall we have too few galaxies and cannot rival the dense sampling of the flow which has been achieved with nearby spirals. For studies of the Hubble flow out to 2500 km s^{-1} or so, those methods have significant advantages over anything that relies on the ellipticals. This is well illustrated by comparing our sample of ellipticals (Fig. 1) with the distribution of bright galaxies on the sky (Fig. 2). The great strength of the supergalactic band is almost completely due to bright spirals. Our data set is at its best in the 2000–7000 km s^{-1} velocity range. Finally, our choice of ellipticals measures the peculiar velocities in atypically dense regions.

There have been many pioneering studies on the uniformity of the Hubble flow beyond the Virgo region: for example, Rubin, Ford, and Rubin (1973) and Rubin *et al.* (1976*a*, 1976*b*), whose work was followed by Peterson and Baumgart (1986) and by Collins, Joseph, and Robertson (1986); Aaronson *et al.* (1982*a*, hereafter AHMST) and Aaronson *et al.* (1982*b*); de Vaucouleurs and Olson (1982); de Vaucouleurs and Peters (1984, 1985); Hart and Davies (1982); Staveley-Smith (1985); Aaronson *et al.* (1986, hereafter ABMHSC); Shaya (1984); Tully and Shaya (1984); Tammann and Sandage (1985); Lilje, Yahil, and Jones (1986); and we regard our work as a further development of the themes developed previously, particularly in the last five references listed above.

c) *Outline of This Paper*

In § II we discuss our distance indicator and the corrections for absorption, K-term, $(1 + z)^4$ dimming, and cosmological effects. Malmquist corrections to both distances and distribution functions are derived, and the Coma cluster is used as a standard to place our relative distances onto a scale in velocity units.

In § III we determine the best slope, x, in the $D_n - \sigma^x$ relationship and the error in ln (distance) of one galaxy based on the scatter in that relationship.

Section IV rejects galaxies with inaccurate distances or inadequate data and gives a series of maps showing the departures of galaxy motions from perfect Hubble flow. It identifies regions of the sky in which there appear to be systematic departures.

Section V and Appendix C give a general discussion of maximum-likelihood methods of fitting model velocity fields to such data and show how various other methods, such as width schemes, are related to the Malmquist-corrected distribution-

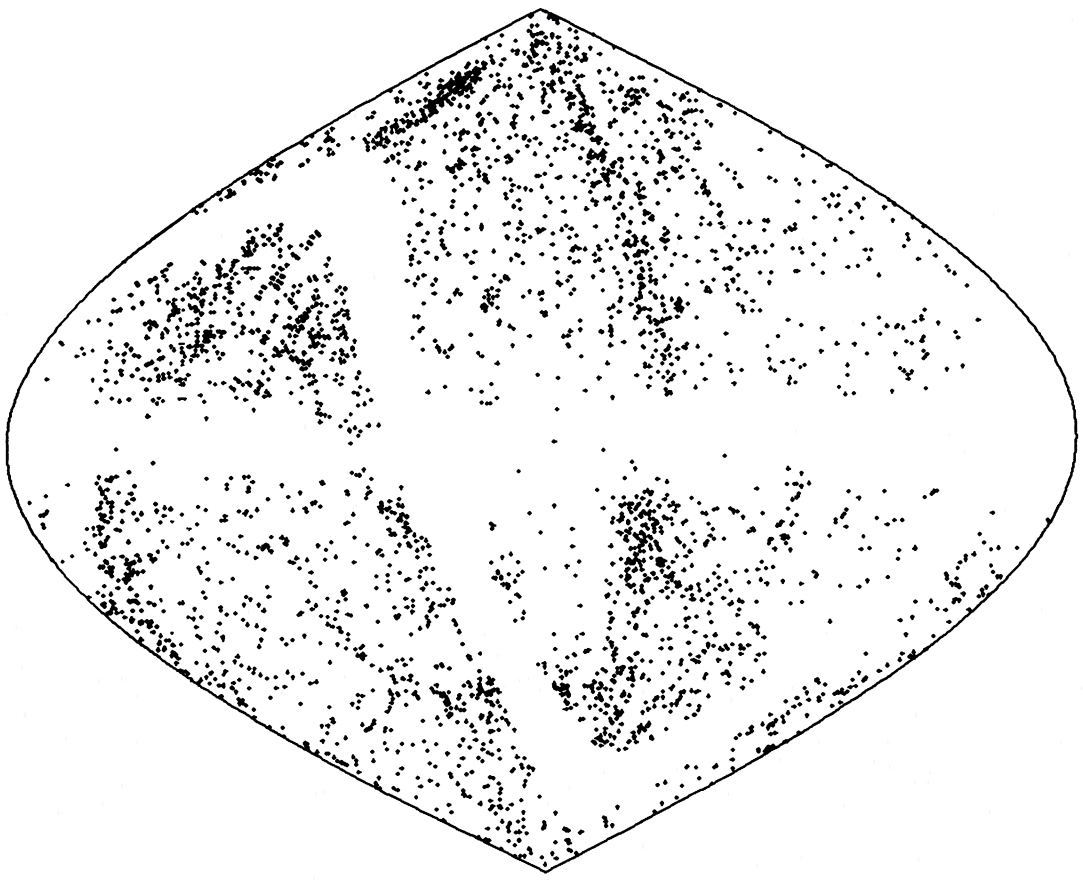

FIG. 2.—The sky distribution of bright galaxies in the UGC and ESO catalogs, coordinates as in Fig. 9

function fitting that we adopt. We show how to deduce both the best-fitting model and its errors and how to generalize to Virgo flow models, anisotropic Hubble expansion, and flows dominated by massive, distant concentrations of matter.

Section VI discusses the results of such model fitting and demonstrates that the best-fitting Hubble expansion of the whole sample of elliptical galaxies has a zero point that is moving some 521 km s^{-1} with respect to the local microwave zero point. This result is not sensitive to any imposed Virgo inflow velocity. We also get the same bulk flow in nearby distance shells but not in those beyond $\sim$3500 km s^{-1}. Quadrupolar variations in the Hubble flow are detectable and suggest that the motion could arise from a mass concentration at between 4000 and 5000 km s^{-1}. When we explore models that include inflow toward such a massive concentration, no extra bulk flow is needed. The Centaurus clusters move rapidly with the flow and lie in the foreground of the massive concentration to which the flow is directed.

Section VII rediscusses error estimates, taking account of the correlations between galaxies and looking for possible causes of systematic errors such as sensitivity to photometric zero points and to errors in the absorption corrections.

In § VIII we provide evidence that we can see the mass concentration that causes the motion and dominates other features of the supergalactic plane in both light and gravity. This justifies the name supergalactic center. We estimate the distance, size, mass, and velocity dispersion and compare them to those of other large superclusters.

In § IX we compare our main result with others published in the literature. A re-reduction of all such data and a more extended discussion will be published separately (Burstein *et al.* 1988).

In § X we look at interpretations of our result and its implications for density fluctuations in the universe.

II. NATURE OF THE DISTANCE INDICATOR

a) Introduction

If a given galaxy is seen from different distances, its angular diameter decreases as $1/r$. Hence, for one galaxy, $1/D_n$ is a measure of its distance. Looking at the galaxies of different diameters in the Coma cluster we found the empirical relationship $D_n \sim \sigma^{1.33}$ (Dressler *et al.* 1987*b*). The same form of law holds also among galaxies in the Virgo cluster and among all other clusters for which we have data. As discussed later, the slope of the line that minimizes the scatter in the distance-dependent quantity $\log D_n$ at each $\log \sigma$ is 1.2 ± 0.1. This leads us to use $\sigma^{1.2}/D_n$ as a distance indicator for any elliptical galaxy. In practice, low-σ ellipticals show large scatter, so we restrict use of this distance indicator to galaxies with $\log_{10} \sigma \geq 2.0$, that is $\sigma \geq 100$ km s^{-1}.

It is essential that the angular diameter D_n always be measured to the same point within a galaxy independently of how far away that galaxy is or at what velocity it moves. To this end we define D_n as the angular diameter of that circle within which the integrated surface brightness of the galaxy is $\Sigma = 20.75$ mag arcsec^{-2} in the B photometric band. This threshold is to be applied to the integrated light per unit area *after* correction for interstellar absorption, K-correction for redshift of observing window, and $(1+z)^4$ correction for Doppler and aberration dimming (see Appendix A).

A given slit size in arcseconds gives different sizes when projected into galaxies at different distances. Since the velocity dispersion in an elliptical galaxy varies with distance from the center, the observed velocity dispersion is given a small aperture correction to allow for this (Davies *et al.* 1987). (An analogous correction is also made to the Mg_2 indices, which are used briefly below.) All velocity dispersions are measured after transforming to a logarithmic wavelength scale, which yields the dispersion in the galaxy rest frame independent of radial velocity.

Although the corrected surface brightness and sigma are independent of distance and cosmology, they are not independent of viewing angle for nonspherical galaxies. However, it can be shown using the tensor virial theorem (Faber *et al.* 1987) that the combination $\sigma^{1.2}/D_n$ is approximately independent of aspect angle, so that aspect effects are expected to introduce negligible scatter into the distances. The clusters confirm this in that the distance residuals do not correlate with axial ratio. The major sources of scatter appear to be observational errors and intrinsic differences in M/L, both of which contribute about equally (Faber *et al.* 1987). The latter set an absolute limit to the accuracy for distances to elliptical galaxies of $\sim$17%, beyond which it does not appear possible to improve the current distance indicator without determining M/L differences independently.

We make a small correction to the distances derived above, which allows for the fact that in cosmological models the apparent diameter does not decrease linearly with redshift. For details see Appendix A.

b) Malmquist Bias in Estimated Distances and Velocities

The raw distance estimates are biased because there are greater numbers of galaxies in the universe at greater distances. This implies that, within a given range of estimated distance, more will have been scattered by the errors down from larger distances than up from smaller ones. This bias is similar in origin to the familiar Malmquist bias in magnitude-limited samples, and for this reason we refer to it by the same name. Notice that the true spatial distribution of the population enters the argument from the very beginning. Throughout this paper we estimate Malmquist effects with the null hypothesis that galaxies are uniformly distributed. Then Malmquist corrections are 15% on single galaxies and are less for galaxies in groups by a factor $1/N$.

Departures from uniformity give extra effects of the same magnitude, but of opposite signs, on the near and far sides of any concentration. Malmquist effects toward Centaurus are further discussed in § VII*b*.

The basic distance indicator is the σ-D_n relationship, which we model as a power law: $D_n \propto \sigma^x$ (Dressler *et al.* 1987*b*). The estimated ln (distance), l_e, is therefore given by

$$l_e = x \ln \sigma - \ln (D_n) + \text{constant} . \qquad (2.1)$$

The problem of determining the best slope and zero-point in this relation is discussed in Appendix B.

Let Δ be the dispersion in $\ln D_n$ at measured σ for the galaxies in a cluster. We can estimate typical values of Δ by taking means over several clusters, and we shall find later that this scatter is the same for field galaxies. Taking the scatter in our estimated ln (distance) to be distributed Gaussianly about the true value $l = \ln r$, the probability distribution of l_e given l is

$$p_0(l_e \mid l) = (2\pi\Delta^2)^{-1/2} \exp\left[-\tfrac{1}{2}(l - l_e)^2/\Delta^2\right] . \qquad (2.2)$$

In practice we are faced with the inverse problem of finding l

when l_e has been measured. Let $n(r)dr/r$ be the number of field galaxies within the observing cone in range dr. For a power law n,

$$n\frac{dr}{r} \propto r^{\alpha-1}\,dr \propto e^{\alpha l}\,dl\,, \tag{2.3}$$

so that a uniform distribution has $\alpha = 3$. Then the distribution of l for given l_e is

$$p_1(l\,|\,l_e) = p_0\,e^{\alpha l}\Big/\int p_0\,e^{\alpha l}\,dl$$
$$= (2\pi\Delta^2)^{-1/2}\exp\{-\tfrac{1}{2}[l-(l_e+\alpha\Delta^2)]^2/\Delta^2\}\,. \tag{2.4}$$

Hence l is distributed Gaussianly with its average value $\langle l\rangle = l_e + \alpha\Delta^2$. Since we have a spread in l it is no surprise to learn that the average distance is not the exponential of the average ln (distance). The average distance of a galaxy of estimated distance r_e is

$$\langle r\rangle = \int r p_1(l\,|\,l_e)dl = r_e[1+(\alpha+\tfrac{1}{2})\Delta^2]\,. \tag{2.5}$$

For the uniform distribution, $\alpha = 3$, this demonstrates the mean Malmquist correction to distances of $3.5\,\Delta^2 r_e$ and to ln (distances) of $3.0\,\Delta^2$.

For galaxies in groups or clusters of N members we replace the distance estimates by their median and then replace Δ^2 by Δ^2/N in the above formulae (see Appendix B for further discussion of group distances).

We now consider Malmquist corrections to the velocity distribution of galaxies taking part in the Hubble flow, $v = Hr$. Let the velocity dispersion of field galaxies about this flow field be σ_f. Then the radial velocity distribution at distance r is

$$f(v\,|\,r) = (2\pi\sigma_f^2)^{-1/2}\exp\,[-\tfrac{1}{2}(v-Hr)^2/\sigma_f^2]\,. \tag{2.6}$$

We correct this so as to use our estimated distance r_e rather than the true distance r. To do this we weight with $p_0\,e^{\alpha l}$ just as in equation (2.4), so the velocity distribution of galaxies at estimated distance r_e is

$$F(v\,|\,r_e) = \int f e^{\alpha l}p_0\,dl\Big/\int e^{\alpha l}p_0\,dl\,, \tag{2.7}$$

where as before $l = \ln r$ and $\alpha = 3$ for a uniform distribution. It is useful to define distances and distance estimators calibrated in the units of km s^{-1} since these are independent of the Hubble constant. Thus, in place of r_e we use R_e, where

$$R_e = Hr_e = He^{l_e}\,. \tag{2.8}$$

R_e is the estimated distance converted into km s^{-1} in the Hubble flow.

When equation (2.6) is inserted into equation (2.7) and the integrations are performed (Appendix D), the result is well approximated by

$$F = (2\pi\sigma_e^2)^{-1/2}\exp\,[-\tfrac{1}{2}(v-R)^2/\sigma_e^2]\,, \tag{2.9}$$

where

$$\sigma_e^2 = \sigma_f^2 + R^2\,(\exp\Delta^2 - 1) \tag{2.10}$$

and

$$R = R_e\exp\,[(\alpha+\tfrac{1}{2})\Delta^2]\,. \tag{2.11}$$

Notice that the effective velocity dispersion σ_e is significantly greater than σ_f at large R_e due to distance errors. This is because galaxies at different true distances and Hubble velocities can have the same estimated distance. Notice also that the Malmquist correction term in R means that in terms of R_e the effective Hubble constant is larger by the exponential factor in equation (2.11).

$F(v\,|\,R_e)$ gives us the probability that a galaxy at estimated distance R_e has radial velocity v.

III. SLOPE AND ZERO POINT OF THE σ-D_n RELATIONSHIP

Two approaches are possible to determining the slope and zero point of the σ-D_n relationship, (1) calibrating the relationship from cluster galaxies, which are presumed to be at the same distance, or (2) determining the constants simultaneously with fitting a model to the velocity field. We adopt the first approach as it can be shown (Appendix C) that the second may result in biased values for both the constants and the velocity model. A first step towards calibrating the distance relation was presented in the paper by Dressler *et al.* (1987*a*), which discussed a subset of the data on seven clusters and established that the σ-D_n relation is an improved distance indicator over L-σ^4. We have now merged these initial cluster data with our general data and here give final values for the best slope and zero point based on all suitable clusters.

From 10 clusters with five or more members, we find a mean slope in $D_n \sim \sigma^x$ of $x = 1.20$. The details of the individual cluster fits are given in Appendix B. This slope differs from the value 1.33 given in Dressler *et al.* because it is the regression of D_n on σ, rather than the "true" slope, as explained in the Appendix.

All distances, R, in this paper are expressed in units of km s^{-1}, which bypasses the usual Hubble constant. However, the model distance scale still has to be adjusted such that, in the mean, $R = v$ for all galaxies. We have found it convenient to adopt the distance to Coma as a fiducial starting point. If Coma were at rest with respect to the microwave background (CMB), its observed radial velocity corrected to microwave rest (7200 km s^{-1}) would fix the velocity that corresponds to unit length. Later refinements to our modeling allow Coma to move and give it a small peculiar velocity, -260 km s^{-1}. This correction plus the median observed value of [1.2 log σ − log D_n] for Coma yield the following expression for the raw estimated distance for individual galaxies (R_e and σ in km s^{-1}, D_n in units of 0.1):

$$2.303l_e = \log R_e = 1.20\log\sigma - \log D_n + \log\left(\frac{1+7/4z}{1+7/4z_{\rm Coma}}\right) + 1.411\,. \tag{3.1}$$

The cosmology correction is the term in parentheses and is taken relative to Coma, as explained in Appendix A. Details of the zero-point derivation are given in Appendix B. The precise zero point depends on the peculiar velocity adopted for Coma and therefore changes slightly from model to model.

Equation (3.1) is correct for individual galaxies but is biased for groups, because the sampling in them is usually diameter limited. The reason for this bias and the derivation of the necessary correction are described in Appendix B. The effect can amount to a +10% correction in distance for groups at 6000 km s^{-1}.

The magnitude of the measuring error, Δ, per galaxy can be estimated from the rms scatter within groups. Estimates of Δ for the 10 richest clusters are given in Appendix B. A weighted

rms average for all groups with two or more members (251 galaxies) gives $\Delta = 0.22$. Deleting Abell 2199 and DC 2345−48, the two clusters which have the most scatter, reduces this to 0.20. We also have an independent estimate of Δ from the maximum-likelihood flow model using the whole sample, as described in § VI*b*. This agrees well and yields $\Delta = 0.21$. We conclude that the errors in the D_n-σ relation are well understood and adopt $\Delta = 0.21 \pm 0.02$.

Evidence that the Malmquist correction is both necessary and accurate is shown in Figure 3, which plots the residual $v - R$ versus v radial velocity. Groups and individual galaxies are solid and open circles. The upper panel (Fig. 3*a*) shows the raw distances before Malmquist correction. The median residual should be zero, but for the open circles it floats upward at larger redshifts. The filled circles do not show a strong effect because the bias is proportional to Δ^2/N (eq.

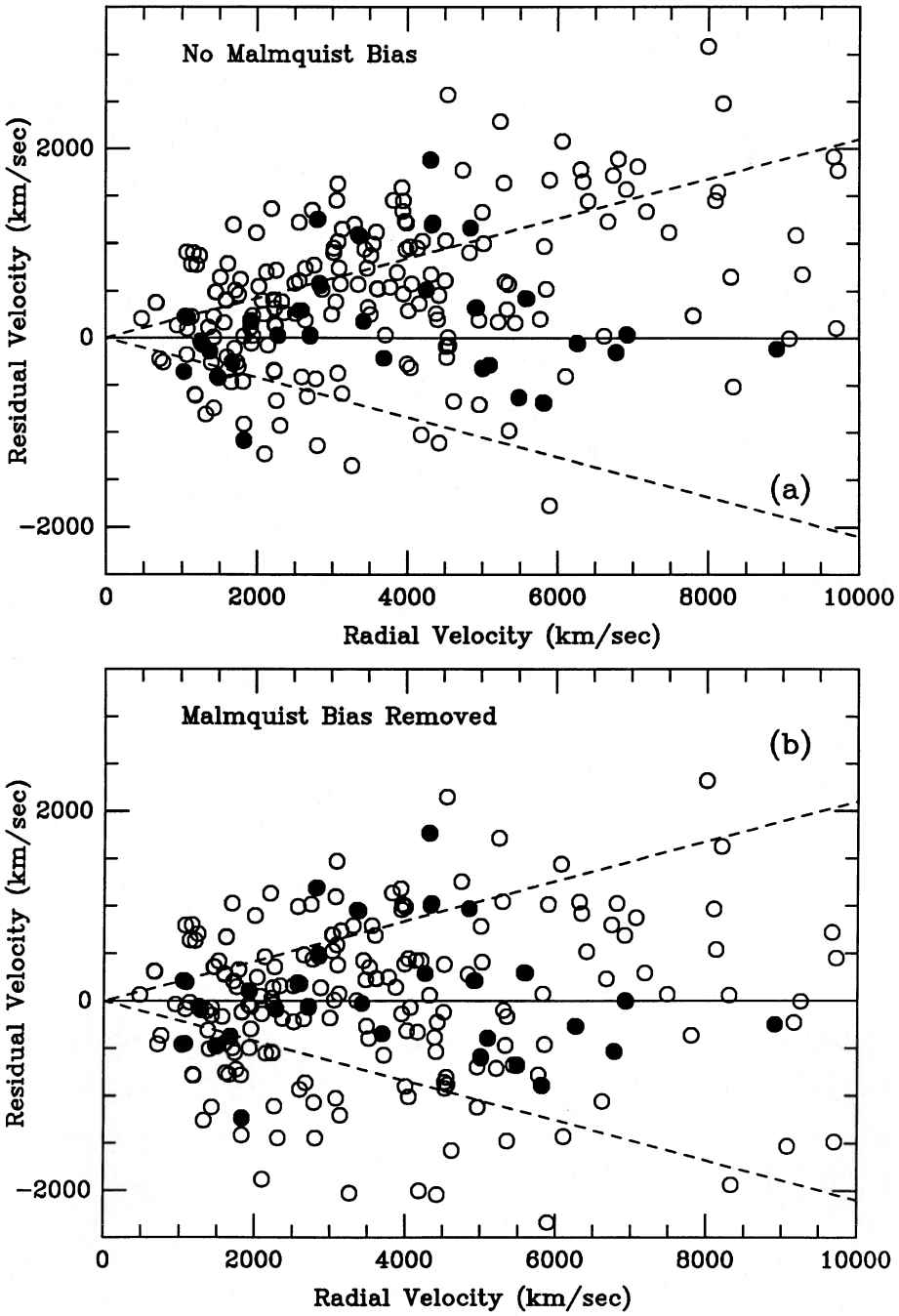

FIG. 3.—The residual velocities of groups (those aggregates with three or more members, *filled circles*) and individual galaxies (*open circles*) plotted as a function of radial velocity with respect to the Local Group (*a*) before the distance estimates are Malmquist corrected and (*b*) after Malmquist correction. The dashed lines indicate the expected 1 σ scatter due to an uncertainty in distance of $\pm 21\%$ per galaxy assuming a uniform Hubble flow. Note that distances to individual galaxies are systematically underestimated when no Malmquist bias correction is applied resulting in systematically positive residual velocities. A few groups with $2500 < v < 4300$ km s^{-1} have high residual velocities after Malmquist correction; these represent real peculiar velocities rather than distance errors (*see text*). In (*b*) the five remaining groups with strongly positive residuals belong to the N1600–1700 and Centaurus regions and are believed to show real deviations.

[2.11]). Application of the correction brings the two classes into agreement (Fig. 3*b*). Many of the remaining group residuals are thought to be due to real motions.

A Malmquist correction as in equation (2.11) merely changes H_0 if the error per object is constant. As noted in § II*b*, this introduces a constant scale change for every galaxy, which is normalized out. The correction becomes vitally important, however, when the error per object is variable, as is the case here for groups versus single galaxies. For equation (2.11) to be valid we must ensure that distance errors Δ are uniform over the whole sample. Our observing procedures were designed to give the same accuracy on all objects independent of brightness. A check on Δ versus distance using clusters and the maximum-likelihood method reveals no statistically significant trend. The evidence is therefore good that the data set is statistically homogeneous and that a Malmquist correction using a uniform Δ is valid.

For convenience we collect together here a summary of all the corrections made to the data:

1. Spectra placed on a logarithmic wavelength scale to yield σ in rest frame of each galaxy;
2. Aperture correction to σ and Mg_2;
3. Interstellar absorption correction to aperture magnitudes;
4. K-correction to aperture magnitudes;
5. $(1 + z)^4$ correction to aperture magnitudes;
6. $(1 + 1.75z)$ correction to predicted distances;
7. Malmquist correction to predicted distances;
8. Diameter-bias correction to group distances.

IV. THE OVERALL VELOCITY FIELD

a) Elimination of Unreliable Data

Only galaxies whose D_n values are of quality 2 or better (error ≤ 0.05 dex; Burstein *et al.* 1987) are used. Of them, 433 have measured velocity dispersions.

Galaxies with velocity dispersions less than 100 km s^{-1} show significantly greater scatter in almost all correlations. We therefore eliminated all 25 of them from the final data set. At least some of these have significant measurement errors.

Several galaxies with effective surface brightness higher than $19^m.5$/arcsec^2, such as M32 and NGC 4486B, are believed to be stripped satellites. Our distance estimates are systematically too large for them so we have dropped all nine such from further analysis; of these, three were already eliminated above.

NGC 3759 ($V_H = 5577$ km s^{-1}) and NGC 1595 ($V_H = 4725$ km s^{-1}) show residuals greater than 3 σ in all our solutions. We did not take spectra of 3759; it is one of the two galaxies whose dispersions were taken from the literature and so may have different errors. If kept in the discussion, its 3.45 σ deviation would make a contribution to the least-squares solution 12 times that of a typical galaxy. This is too high when its dispersion of 112 km s^{-1} is only just over our reliability limit and its error may be larger than typical. We have therefore dropped it from discussion altogether.

NGC 1595's contribution is 13 times that of a typical galaxy. It has the low velocity dispersion of 119 km s^{-1}, but this is the average of two concordant AAT spectra that give 117 and 121 km s^{-1}, and its photometry is first class. Its velocity deviation is 2000 km s^{-1} outward and it lies toward $l = 254$, $b = -42$ so it has little influence on the component of the motion toward Centaurus. We have omitted it from our reductions because we wish to establish our result without appeal to such a high weight given to an individual galaxy. Including it increases the flow velocity by 14 km s^{-1} and shifts the mean flow direction a few degrees to $l = 304$, $b = 6$, all well within the errors of our solution.

b) Pictures of the Velocity Field

In perfect Hubble flow, the radial velocities measured with respect to the microwave (CMB) zero point would be linear functions of distance. We put our distances R into velocity units as discussed in § III. If these distances are subtracted from the radial velocities in the CMB frame, we should get zero. Due to errors, $v - R$ may be nonzero, but it should be random with no systematic trends. Any systematic behavior should be attributable to perturbations from smooth Hubble flow, such as that due to the gravity of the Virgo supercluster causing deceleration of the expansion around Virgo.

For galaxies in a plane, one can picture the field of their perturbed radial velocities by placing a dot at R and extending it with a line in the radial direction of length $v - R$ (see Fig. 4). To emphasize the sense of these motions, it is convenient to represent outward-perturbed velocities by solid lines and inward-perturbed velocities by dotted ones. In practice, the galaxies do not lie in a plane, so it is necessary to adopt some projection procedure. We choose a particular plane through us defined by the direction of its normal in the sky (a pole of its great circle). We take all galaxies in directions within $22^\circ.5$ of that plane and plot their distances and $v - R$ lines as though they lay in the plane itself. Thus all galaxies at distance R are plotted at distance R from the origin, although in extreme cases they may be separated in the sky by a "latitude" shift of up to 45°. By rotating the pole chosen for the plane in 45° steps, we can cover the whole sky with four such figures. These figures show velocities relative to the CMB. Figure 4*b* shows such a plot for galaxies within $22^\circ.5$ of the supergalactic plane.

In Figures 4*a*–4*d* the principal plane of each plot is rotated successively by 45° about the line in which the supergalactic plane meets the Galactic plane, i.e., $l = 317$, $b = 0$. This axis is chosen as the X-axis of each plot. The Galactic coordinates l, b of one pole of the plane are written at each top-right-hand corner.

Careful perusal of Figure 4 shows that almost all arrows close to a horizontal double-ended cone point from left to right. This indicates that the galaxies are not at rest in the frame of the microwave background but have a systematic streaming motion.

A clearer demonstration of this motion of ellipticals relative to the CMB frame is given in Figures 5*a* and 5*b*. These plot galaxy or group peculiar velocities relative to the CMB frame against the cosine of the angle between the galaxy's direction and the direction of average motion. A uniform bulk flow would give a straight line through the origin whose intercept at $\cos \vartheta = 1$ would be the bulk velocity. Slopes are seen in the data from the near and intermediate distances covered by Figures 5*a* and 5*b*, but the weaker slope of Figure 5*c* is confused by the increased scatter at those larger distances. There is evidence for a nonuniform slope in Figure 5*b*, which shows a turned-up end beyond $\cos \vartheta = 0.8$.

The scatter in these figures, particularly in Figures 5*a* and 5*b*, is larger than the observational errors. In addition to large-scale systematics, there are also motions on smaller scales. We model both large-scale and small-scale motions in the next section.

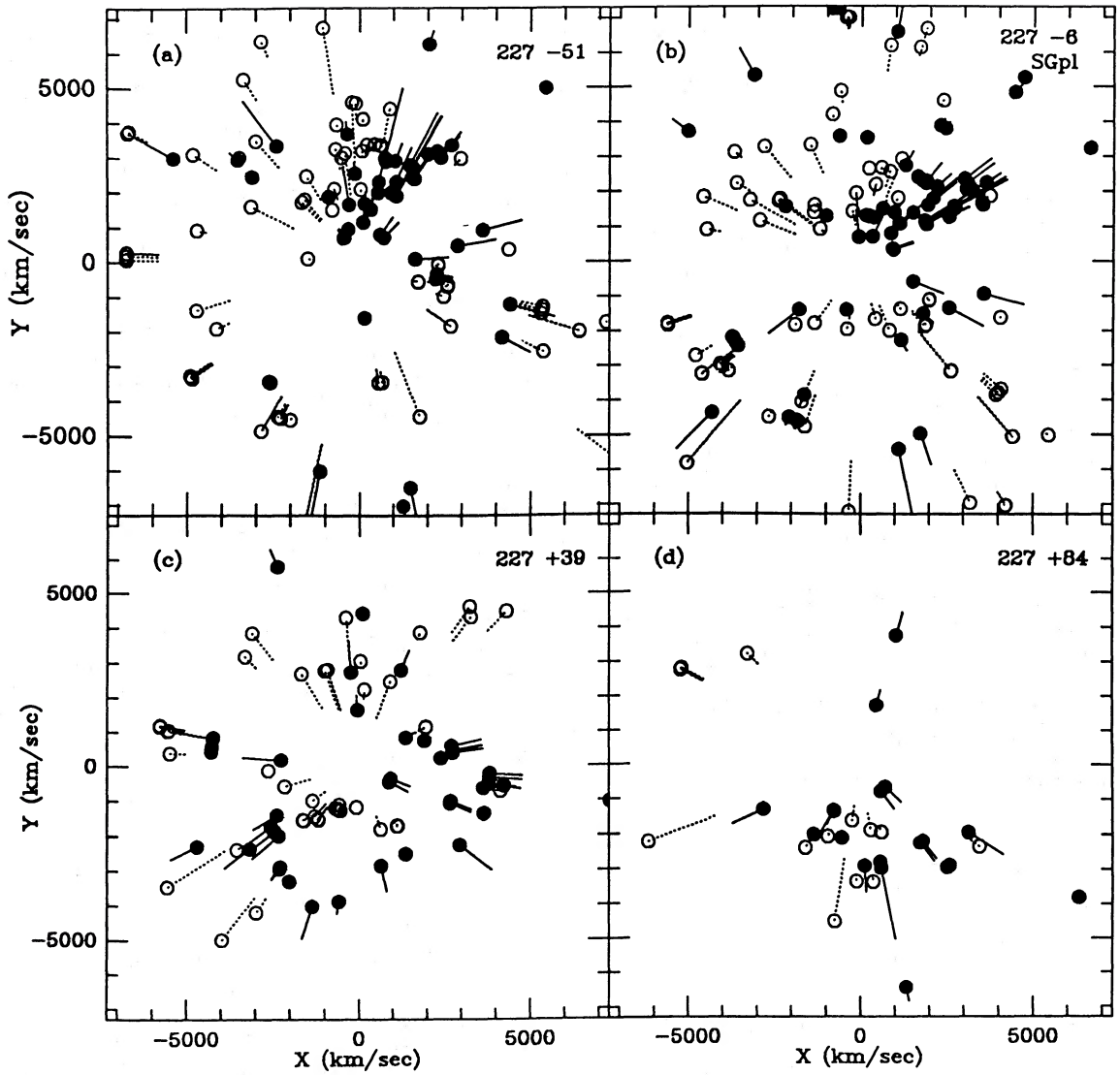

FIG. 4.—Peculiar radial velocity vectors of elliptical galaxies within 22°.5 of each principal plane. Each galaxy is placed at its distance R and a line of length $v - R$ is drawn ending at v, the radial velocity in the CMB radiation's rest frame. Outward moving points are filled. The x-axis lies toward $l = 317$, $b = 0$, the line in which the Galactic plane meets the supergalactic plane. (*a*)–(*d*) The y-axis is rotated about the x-axis by 45° to get from one figure to the next; (*b*) has all galaxies within 22°.5 of the supergalactic plane. The l, b direction of the normal to each principal plane is given in the top right-hand corner of each plot.

V. MODELING THE VELOCITY FIELD

Appendix C discusses methods of analyzing the data. We adopt the maximum-likelihood velocity distribution for galaxies at a given *estimated* distance. This method gives unbiased estimates of the velocity field and needs no sample incompleteness estimates.

a) Model Parameters

Given the observed directions of the elliptical galaxies, $\hat{\boldsymbol{r}}$, and their estimated distances, R_e, the probability of finding their heliocentric velocities v is the product over all objects of the distributions (eq. [2.7]),

$$P = \Pi F(v \mid R_e) , \tag{5.1}$$

and the likelihood of the observed distribution is (see eq. [2.9])

$$L = \ln P = -\sum [\tfrac{1}{2} \ln (2\pi\sigma_e^2) + \tfrac{1}{2}(v + \boldsymbol{v}_0 \cdot \hat{\boldsymbol{r}} - R)^2/\sigma_e^2] , \tag{5.2}$$

where the sum extends over all objects observed and σ_e depends on the object concerned through R_e. In equation (5.2) and hereafter, v is the observed heliocentric radial velocity of a galaxy whose direction is given by the unit vector $\hat{\boldsymbol{r}}$. The velocity of the galaxy relative to the frame in which the motions of our sample are best fitted by a Hubble law is $v + \boldsymbol{v}_0 \cdot \hat{\boldsymbol{r}}$, where $\boldsymbol{v}_0$ is the velocity of the Sun in that frame. Together, these terms make up the velocity relative to the idealized flow, called v in equation (2.9). To find the best estimate of $\boldsymbol{v}_0$ we maximize L over all choices of $\boldsymbol{v}_0$. Likewise, to find the best estimate of any other parameter of the assumed distribution such as σ_f, we maximize L over all choices of it. The estimated errors of the values so obtained are found by seeing how L decreases away from the maximum. Thus, the errors in $\boldsymbol{v}_0$ are described by the tensor $\partial^2 L/\partial \boldsymbol{v}_0 \, \partial \boldsymbol{v}_0$, and its principal axes give the inverse variances of the errors in $\boldsymbol{v}_0$ in those directions. We use Cartesian Galactic coordinates x towards the Galactic center, y toward Galactic rotation, and z toward the north Galactic pole.

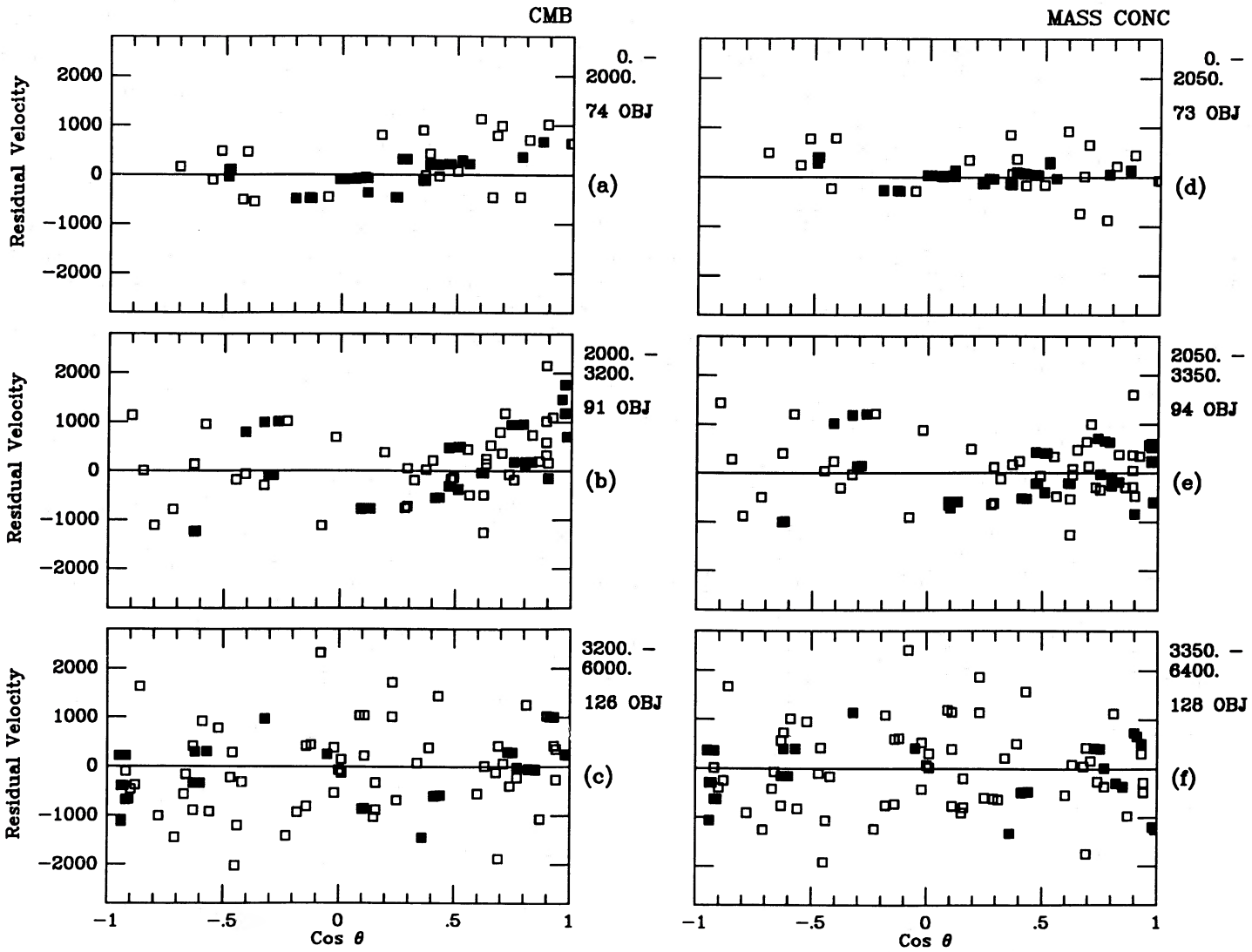

FIG. 5.—The peculiar velocities of groups (*black squares*) and individual galaxies (*white squares*) plotted as a function of the cosine of ϑ, the angle between the streaming motion $l = 307$, $b = 9$, and the direction of the galaxy. A bulk flow over and above Hubble expansion would show a linear slope in these plots. (*a*) Objects with distances $R_e \leq 2000$ km s^{-1}; velocities in the CMB frame. (*b*) Objects with distances $2000 < R_e \leq 3200$ km s^{-1}; velocities in the CMB frame. (*c*) Objects with distances $3200 < R_e \leq 6000$ km s^{-1}; velocities in the CMB frame. (*d*)–(*f*) As (*a*)–(*c*) but plotting residual peculiar velocities after subtracting the flow generated by the massive concentration and Virgo.

Each group of galaxies is included in the sum (5.2) and treated as a single object. Such groups have more accurate distances based on medians, so the distance errors are decreased from Δ to $\Delta/(N)^{1/2}$. However, we take the velocity dispersion in the velocities of the group barycenters to be σ_f, the same as for the field galaxies. This reflects our belief that these motions are gravitationally induced on a large scale so that accelerations are independent of mass. We find evidence that σ_f for groups is indeed the same as for the whole sample in § VI.

The point of summing in equation (5.2) over objects rather than individual galaxies is that those in a group are not statistically independent and the group as a whole gives only *one* sample of the large-scale deviant velocity field, not N. However, N does increase the accuracy of that sample. The formula for the σ_e^2 of a group is

$$\sigma_e^2 = \sigma_f^2 + R^2[\exp(\Delta^2/N) - 1] .$$

At large R, where the second term dominates and when Δ^2/N is small, we find

$$1/\sigma_e^2 = N/(R^2\,\Delta^2) ,$$

so in that limit the group acts like N independent objects. However, in the opposite limit, when σ_f^2 dominates, each group has a weight of only σ_f^{-2} independently of its N.

Maximizing L over all choices of $\boldsymbol{v}_0$ gives us the equation

$$\partial L/\partial \boldsymbol{v}_0 = 0 = \sum (v + \boldsymbol{v}_0 \cdot \hat{\boldsymbol{r}} - R)\hat{\boldsymbol{r}}/\sigma_e^2 \qquad (5.3)$$

and hence

$$\mathbf{M} \cdot \boldsymbol{v}_0 = U, \qquad (5.4)$$

where

$$\mathbf{M} = \sum \hat{\boldsymbol{r}}\hat{\boldsymbol{r}}/\sigma_e^2 \qquad (5.5)$$

and

$$\boldsymbol{U} = -\sum (v - R)\hat{\boldsymbol{r}}/\sigma_e^2 . \qquad (5.6)$$

Evidently the best value of $\boldsymbol{v}_0$ is given by

$$\boldsymbol{v}_0 = \mathbf{M}^{-1} \cdot \boldsymbol{U} . \tag{5.7}$$

The errors in this estimate are given by σ_1, σ_2, and σ_3, where σ_1^2, etc. are the principal values of $\mathbf{M}^{-1}$. Notice that

$$\boldsymbol{M} = \partial^2 L / \partial \boldsymbol{v}_0 \, \partial \boldsymbol{v}_0 \tag{5.8}$$

We can, of course, restrict consideration to elliptical galaxies in any particular distance range we choose. We can therefore study $\boldsymbol{v}_0$ and its errors as a function of the distances of the galaxies.

b) *Modifications*

It is simple to modify the above procedure for different models. The order of evaluation of the new parameters is outlined in Table 1. Four modifications are considered:

1. Allowance for the fact that the distance scale based on Coma may not be the best;
2. Allowance for a quadrupole anisotropy in the Hubble flow, so that in place of $\boldsymbol{v} = H\boldsymbol{r}$ we have $\boldsymbol{v} = \mathbf{H} \cdot \boldsymbol{r}$;
3. Allowance for a Virgo infall;
4. Allowance for a large-scale infall to explain the deviation of the observed velocity field from that defined by the cosmic microwave radiation.

The first modification is achieved by writing hR for R in equation (5.2). Maximizing L over all choices of h, the modification to the distance scale, yields the equation

$$\Sigma(v + \boldsymbol{v}_0 \cdot \hat{\boldsymbol{r}} - hR)R/\sigma_e^2 = 0 , \tag{5.9}$$

and thus

$$h = [\Sigma(v + \boldsymbol{v}_0 \cdot \hat{\boldsymbol{r}})R\sigma_e^{-2}]/\Sigma(R^2\sigma_e^{-2}) . \tag{5.10}$$

The errors in h are likewise easily computed from

$$\sigma_h^2 = 1/\Sigma(R^2\sigma_e^{-2}) . \tag{5.11}$$

TABLE 1

MAXIMUM-LIKELIHOOD PROCEDURE

1. Model heliocentric velocity field by
   i) velocity dispersion σ_f;
   ii) $\boldsymbol{u} = -\boldsymbol{v}_0 + h\boldsymbol{R} + \boldsymbol{V}_v$.
   Model parameters $\boldsymbol{v}_0$, h, σ_f, V_v.
2. Calculate the probability that a galaxy at estimated distance R_e (before Malmquist correction) has a radial velocity v in the above velocity field, the distance estimator having an error Δ.
3. For the standard model $R_e \leq 8000$ km s^{-1}, maximize the probability of finding *all* the galaxies at their observed velocities (given their estimated distances) by varying the parameters, $\boldsymbol{v}_0$, h, σ_f, V_v, Δ. Hence find the peculiar velocity DV_{Coma} of Coma that makes $h = 1$.
4. Compare Δ with the distance spread of members of clusters. Adopt standard values of Δ, σ_f, DV_{Coma}, and Virgo infall.
5. Maximize probability of observed velocities of subsets of the data, shells, groups, etc. to find the best $\boldsymbol{v}_0$ for those subsets.
6. Change $h\boldsymbol{R}$ term in $\boldsymbol{u}$ to $\mathbf{h} \cdot \boldsymbol{r}$ and maximize the probability over the components of $\mathbf{h}$ leaving $\boldsymbol{v}_0$ fixed at the value determined in 5.
7. Add a flow induced by a very massive distant concentration of galaxies designed to give the mean motion of the elliptical galaxies and find what flow magnitude and distance of the concentration give the best fit and what residual bulk flow is needed.
8. Set residual bulk flow to zero [i.e., $\boldsymbol{v}_0 = \boldsymbol{v}_\odot - \boldsymbol{v}_{\text{CB}} = (-13, -242, 289)$] and repeat the maximization over σ_f, Δ, DV_{Coma}, R_m, V_m to find the best model with a massive concentration causing the flow.

c) *General Method for Modeling*

For more general models the method is now clear. We take some model form of flow in the heliocentric rest frame $v = u(\boldsymbol{R}, a, b, c, \ldots)$, where a, b, c, etc. are parameters to be determined. The likelihood is then

$$L = -\Sigma\tfrac{1}{2}[(v - u)^2\sigma_e^{-2} + \ln(2\pi\sigma_e^2)] \tag{5.12}$$

We maximize this likelihood over all choices of the parameters to obtain best estimates, and the second derivatives of L give the matrix that describes the errors in these estimates.

Any fluid flow field, $\boldsymbol{u}(\boldsymbol{r})$, can be expanded about a point, $\boldsymbol{r}_0$, in the form

$$\boldsymbol{u}(\boldsymbol{r}) = \boldsymbol{u}(\boldsymbol{r}_0) + \mathbf{H} \cdot (\boldsymbol{r} - \boldsymbol{r}_0) + \cdots , \tag{5.13}$$

where $\mathbf{H} = \partial \boldsymbol{u}/\partial \boldsymbol{r}$, evaluated at $\boldsymbol{r} = \boldsymbol{r}_0$. Taking $\boldsymbol{r}_0$ to be the position of the Sun, the heliocentric radial velocities in such a flow would be

$$u = \hat{\boldsymbol{r}} \cdot \boldsymbol{u} = \hat{\boldsymbol{r}} \cdot \boldsymbol{u}_0 + \hat{\boldsymbol{r}} \cdot \mathbf{H} \cdot \boldsymbol{r} + \cdots . \tag{5.14}$$

We compare this expression with the flow field that we have already used: $-\hat{\boldsymbol{r}} \cdot \boldsymbol{v}_0 + R$ in equation (5.2). Evidently when $\mathbf{H}$ is a multiple of the unit matrix these expressions are the same provided we identify $\boldsymbol{u}_0$ with $-\boldsymbol{v}_0$ and $H\boldsymbol{r}$ with the final Malmquist corrected estimate, R. To get the more general models we must allow for anisotropies in the Hubble constant. Since $\boldsymbol{r} = r\hat{\boldsymbol{r}}$, equation (5.14) involves only the symmetrical components of $\mathbf{H}$. The antisymmetrical components correspond to rotation rates. They do not give rise to radial velocities and so are not determinable from our data. Henceforth we shall replace $\mathbf{H}$ by its symmetric part and write it $H\mathbf{h}$.

d) *Quadrupole Anisotropy*

As in the first modification described in § V*b*, we replace R in equation (5.2), but now by $\hat{\boldsymbol{r}} \cdot \mathbf{h} \cdot \hat{\boldsymbol{r}}R$ rather than by hR.

Maximizing the resultant L over all choices of the symmetrical components of $\mathbf{h}$ yields the equation

$$\Sigma(v + \boldsymbol{v}_0 \cdot \hat{\boldsymbol{r}} - \hat{\boldsymbol{r}} \cdot \mathbf{h} \cdot \hat{\boldsymbol{r}}R)\hat{\boldsymbol{r}}\hat{\boldsymbol{r}}R/\sigma_e^2 = 0 . \tag{5.15}$$

This is a linear tensor equation in the symmetrical component of $\mathbf{h}$ which is easily solved as follows: For any pair of indices such as those in the symmetric 3×3 matrix W_{jk} defined below, we define a six-vector w_p such that if $p = 1$, 2, or 3, $w_p = W_{pp}$ (unsummed) and $w_4 = (2)^{1/2}W_{12}$, $w_5 = (2)^{1/2}W_{13}$, and $w_6 = (2)^{1/2}W_{23}$. For a symmetric $3 \times 3 \times 3 \times 3$ tensor $\mathbf{S}_{jklm}$, we likewise define a 6×6 matrix s_{pq} by treating the first pair of indices and the second pair of indices just as we did for W_{jk}. These definitions have been chosen so that $\mathbf{S}:\mathbf{W}$ is a matrix whose corresponding six vector is $\mathbf{s} \cdot \boldsymbol{w}$. Now equation (5.15) can be written

$$\mathbf{S}:\mathbf{h} = \mathbf{W} , \tag{5.16}$$

where $\mathbf{S}$ is the $3 \times 3 \times 3 \times 3$ tensor $\Sigma\hat{\boldsymbol{r}}\hat{\boldsymbol{r}}\hat{\boldsymbol{r}}\hat{\boldsymbol{r}}R^2/\sigma_e^2$ and

$$\mathbf{W} = \Sigma(v + \boldsymbol{v}_0 \cdot \hat{\boldsymbol{r}})\hat{\boldsymbol{r}}\hat{\boldsymbol{r}}R/\sigma_e^2 . \tag{5.17}$$

The six-vector equation corresponding to equation (5.16) is

$$\mathbf{s} \cdot \boldsymbol{h} = \boldsymbol{w} , \tag{5.18}$$

where $\boldsymbol{h}$ is the six-vector formed from $\mathbf{h}$. We solve equation (5.18) for $\boldsymbol{h}$:

$$\boldsymbol{h} = \mathbf{s}^{-1} \cdot \boldsymbol{w} . \tag{5.19}$$

Knowledge of the six-vector $\boldsymbol{h}$ gives us the components of the symmetrized tensor, $\mathbf{h}$, from which we can find its eigenvectors

and eigenvalues. These give the anisotropies in the Hubble constant.

The errors in **h** are a fourth-order tensor whose significance is hard to comprehend, so we have adopted a simpler approach. What we really wish to know is whether the Hubble constant is significantly anisotropic or whether the observed anisotropies are just the expected fluctuations due to finite numbers, etc. We can answer this question more easily by asking for the errors in the eigenvalue of the Hubble tensor in the fixed eigendirection defined by the maximum-likelihood **h**. We do this as follows. Let e_1, e_2, e_3 be the unit eigendirections defined by **h** so that **h** is of the form $\mathbf{h} = h_1 e_1 e_1 + h_2 e_2 e_2 + h_3 e_3 e_3$. Now write **h** in this form with e_1, e_2, and e_3 fixed, but allow h_1 to vary. The error in h_1 is $\delta h_1 = (\partial^2 L/\partial h_1^2)^{-1/2}$. In this evaluation h_2 and h_3 are held fixed. We treat h_2 and h_3 similarly. We then look to see if h_1 is within δh_1 of unity and similarly h_2 and h_3.

The procedure in evaluating anisotropies is to solve first for an isotropic model and then use the mean velocity $\boldsymbol{v}_0$ given by that solution as a known to insert into the W equation (eq. [5.17]) (see Table 1). We have not solved simultaneously for $\boldsymbol{v}_0$ and **h**. Our reason for doing this is that dipolar and quadrupolar solutions should be nearly independent anyway. They would be independent for uniform sky coverage because of the orthogonality of dipolar and quadrupolar components over the sky, but due to finite numbers and poor coverage in the Galactic plane, that ideal is imperfectly achieved.

e) *Virgo Flow Models*

There are two fundamentally different methods for calculating the Virgo "infall" (lack of outflow) velocity at the Local Group. One is to compare distance ratios to groups of distant galaxies with their velocity ratios and *interpret* differences as due to infall. This method assumes that the Local Group's peculiar velocity is due purely to the influence of Virgo, which is clearly wrong since it is not in that direction. Here, following Schechter (1980) and more particularly AHMST and Lilje, Yahil, and Jones (1986), we look for the pattern of motion in radial velocities that would be induced by a gravitational Virgo infall. As in § II, $\boldsymbol{v}_0$ is the velocity of the Sun with respect to the best-fitting Hubble flow referred to regions beyond Virgo's influence. The Virgo induced flow, $\Delta\boldsymbol{u}(\boldsymbol{r})$, is, with respect to that distant frame, not the Local Group's.

In linear perturbation theory, the perturbation in the velocity field follows the gravity field, which is given by

$$g = \frac{4\pi G}{r^2}\int_0^r \Delta\rho r^2\, dr\ .$$

Thus for $\Delta\rho \propto r^{-(n+1)}$, both Δu and $g \propto r^{-n}$.

When n is close to 1, as is often considered for clusters, we have $\Delta u \propto r^{-1}$. However, this behavior cannot persist into the nonlinear regime. Close to a large cluster we expect an infall velocity close to $[GM/r]^{1/2}$, and so Δu must behave like $r^{-1/2}$ at short distances. Furthermore, extrapolating $\rho \sim r^{-2}$ to large distances leads to an infinite mass perturbation diverging as r, which seems rather extreme. We have chosen instead an interpolation formula for Δu between $r^{-1/2(n-1)}$ and r^{-n}, which gives radial velocities as seen from Virgo of

$$\Delta u = -V_v(r/r_v)^{-(n-1)/2}\{[c^2 + (r/r_v)^2]/(c^2+1)\}^{-(n+1)/4}\ .$$

Here V_v is the Virgo infall velocity at the Sun and r_v is its distance to Virgo. For $c = 1$ and $n = 2$ we notice that at r_v we have $d \ln \Delta u/d \ln r = -5/4$, while $d \ln \Delta u/d \ln r = -1$ at a distance of $r_v/\sqrt{2}$ from the center of Virgo. It is over comparable distance ranges that studies of the density of galaxies have led others to take an overall value $n = 1$.

f) *Massive Concentration Models*

We shall see presently that our data show a velocity zero some 521 km s^{-1} different from the microwave velocity. To investigate the possibility that a large mass concentration on one side of us has caused this we have looked at the simplest such model in which a massive object at distance r_m has caused a perturbation $|\Delta u| = V_m$ at the Sun. We assume for simplicity that $\Delta u \propto |r - r_m|^{-m}$ over the whole region covered by the data. In the linear regime this corresponds to $\rho \propto r^{-(m+1)}$. We modify $\boldsymbol{u}$ in a way similar to that discussed for Virgo infall, but with the direction $\hat{\boldsymbol{r}}_m$ taken to be that of the large-scale motions relative to the background. One may then maximize the likelihood over all choices of V_m and R_m. After experiment, the model adopted has the power $m = 1$ giving a concentration whose density falls as r^{-2}.

VI. RESULTS OF MODEL FITTING

a) *Bulk-Flow Models*

Table 1 summarizes the steps taken in making a model. Table 2 gives the basic parameters determined from the solutions which include a bulk flow and a Virgo infall fixed at $V_v = 250$ km s^{-1} (and $c = 1$, $n = 2$). The solution in the range $R_e \leq 8000$ km s^{-1}, which we call the standard bulk model, is emphasized in bold type. Columns (1)–(11) contain the following:

Column (1).—Above, estimated distance range, R_e in km s^{-1}, of the galaxies in the solution and, below, the field velocity dispersion used, σ_f.

Columns (2), (3), and (4).—The velocity of the bulk flow with respect to the cosmic microwave background. Equation (5.7) gives the maximum-likelihood solution for $\boldsymbol{v}_0 = \boldsymbol{v}_\odot - \boldsymbol{v}_E$, and this is subtracted from the motion of the Sun relative to the CMB, which is $\boldsymbol{v}_\odot - \boldsymbol{v}_{CB} = 377$ km s^{-1} toward $l = 267$, $b = 50$, or in galactic components $(-13, -242, 289)$. Errors are in parentheses.

Column (5).—The fit of the model to the subset of galaxies in the solution would get still better if the distance scale used were multiplied by h. Notice that $h = 1$ for the standard bulk solution by definition.

Column (6).—Above: the raw rms radial velocity residual with respect to the solution. It is uncorrected for measurement error. Below: the raw rms radial velocity residual with respect to pure Hubble flow in the microwave frame.

Column (7).—Above: $X = \Sigma(v-u)^2\sigma_e^{-4}/\Sigma\sigma_e^{-2}$. Maximization of the likelihood over all choices of σ_f^2 shows that X should be 1 for the best-fitting σ_f. Notice that σ_f has been chosen to make this 1.00 for the standard solution. Below: The improvement in likelihood between the flow as modeled and pure Hubble flow in the CMB frame.

Column (8).—$\chi_m^2 = \Sigma(v-u)^2/\sigma_e^2$ is the χ^2 with respect to the model. χ_0^2 is the same expression evaluated about pure Hubble flow in the CMB frame.

Column (9).—Above: The number of objects (i.e., groups, clusters, and isolated galaxies) used in the solution. Below: The total number of observed galaxies in those objects.

Column (10).—Above: V_m, the velocity induced at the Sun by an imposed mass concentration. Below: R_m the distance (in km s^{-1}) from the Sun of the imposed mass concentration.

TABLE 2

DEVIATIONS FROM COSMIC MICROWAVE–BASED HUBBLE FLOW

R_e / σ_f (km s^{-1}) (1)	$\lvert v_E - v_{CB}\rvert$ (km s^{-1}) (2)	l / δl (3)	b / δb (4)	h / δh (5)	$\sqrt{\langle(v-u)^2\rangle}$ / $\sqrt{\langle(v-R)^2\rangle}$ (km s^{-1}) (6)	X / ΔL (7)	χ_m^2 / χ_0^2 (8)	N_{Gr} / N (9)	V_m / R_m (km s^{-1}) (10)	DV_{Coma} (km s^{-1}) Remarks (11)
Solutions for a Bulk Flow (with $V_v = 250$ km s^{-1}, $c = 1$, $n = 2$)										
≤2000	561	311	26	1.08	411	0.82	45	50	0	−4
365	(133)	(18)	(8)	(0.04)	484	10	65	91	0	...
2000–3200	780	298	−9	1.01	673	1.21	65	58	0	−4
365	(156)	(13)	(9)	(0.03)	834	8	81	88	0	...
≤3200	616	307	11	1.03	576	1.03	117	108	0	−4
365	(101)	(11)	(7)	(0.02)	679	15	147	179	0	...
3200–8000	235	326	−1	0.98	708	0.75	64	90	0	−4
365	(193)	(52)	(39)	(0.02)	(734)	0	64	193	0	...
≤8000	**521**	**307**	**9**	**1.00**	**660**	**1.00**	**186**	**198**	**0**	**−4**
365	**(89)**	**(11)**	**(8)**	**(0.02)**	**708**	**15**	**216**	**372**	**0**	...
≤8000	470	306	8	1.00	670	0.94	166	180	0	−4
365	(99)	(14)	(9)	(0.02)	690	12	190	325	0	$A_B < 0.4$
≤8000	697	281	4	1.01	390	1.00	65	56	0	−4
400	(166)	(13)	(9)	(0.03)	632	6	77	230	0	Groups only
≤8000	531	322	11	1.02	800	1.00	127	142	0	−4
320	(119)	(13)	(10)	(0.02)	816	10	147	142	0	Others
Solutions with a Mass Concentration (and $V_v = 100$ km s^{-1}, $c = 0.5$, $n = 3$, $m = 1$)										
≤8300	106	308	13	1.00	636	1.00	192	198	500	−240
245	(78)	(49)	(31)	(0.01)	744	28	248	372	4200	...
≤8300	**0**	**307**	**9**	**1.00**	**641**	**0.99**	**190**	**198**	**570**	**−260**
250	...	...	...	**(0.01)**	**748**	**27**	**244**	**372**	**4350**	...

Column (11).—Above: The peculiar velocity of Coma in the model (for the standard model this is chosen to make $h = 1.00$). Below: Notes on special solutions.

Our initial expectation is that the elliptical galaxies move with the Hubble flow in the CMB frame, i.e., that $v_E - v_{CB}$ should be zero. However, the value found in the standard bulk solution is 521 km s^{-1}, almost 6 times its probable error of ±89.

The main conclusions to be drawn from Table 2 are as follows:

1. Inclusion of a bulk flow gives a significantly better fit to the data. χ^2 drops by 30 whereas one might have expected a drop of only 3 with 3 new parameters. Likewise the probablity changes by exp (15).

2. Both the whole data set and all shells out to $R_e = 3200$ km s^{-1} (which involve true distances out to ∼3500 km s^{-1}) give very similar magnitudes and directions for the bulk flow at ∼570 ± 60 km s^{-1} toward $l = 307 \pm 11$, $b = 9 \pm 8$. However, the distant shell gives an insignificant fall in χ^2 when the bulk flow is introduced. That flow is smaller and poorly determined but is still close to the same direction.

3. The introduction of a flow model gives only modest falls in residual velocities because these are generally dominated by distance errors. However, there is a significant fall in residual velocities for groups, as their distances are more precise (Table 2, row 7, column [6]).

Table 3 gives further details of selected solutions of Table 2. The columns are as follows:

Column (1).—Distance range in km s^{-1}.

Column (2).—Components of the motion of the Sun relative to the frame defined by the motion of the elliptical sample, followed by their errors. The components are in Galactic coordinates with x toward the Galactic center, y toward Galactic rotation, and z toward the north Galactic pole.

Column (3).—Like column (2), but in magnitude and direction.

Column (4).—The Local Group's motion relative to the frame defined by the elliptical galaxy sample.

Columns (5), (6), and (7).—The magnitudes and directions of the principal axes of the Hubble tensor. A value less than 1.0 corresponds to a slow expansion direction; a value greater than 1.0 corresponds to a rapid expansion direction. Both are measured after the shift of frame to that of the sample's motion. For these expansion rates, antipodean directions are equivalent, so (334, 27) is equivalent to (154, −27).

The main conclusion to be drawn from Table 3 is that significant anisotropy exists in the local Hubble flow with a rapid expansion axis directed toward $l = 336$, $b = 18$ and a magnitude close to 1.25 ± 0.06. This may be compared with the quadrupole found by Lilje, Yahil, and Jones (1986) from spiral data, which yield a long axis of 1.15 ± 0.04 toward $l = 308 \pm 13$ and $b = 13 \pm 9$. The good agreement between these in both magnitude and direction adds credence to their reality. It is significant that both directions are close to that of the bulk motion of ellipticals relative to the CMB: $l = 307 \pm 11$, $b = 9 \pm 8$.

An aligned quadrupole is the signature of inflow toward a localized source of gravity. Further evidence for an inflow rather than a uniform streaming comes from dividing the sky into cones about the direction of mean motion. We look at the mean motions determined from different cones. A uniform streaming should give the same result for each cone; in fact, a cone of 60° semiangle directed at the motion in Centaurus yields a mean flow of 913 ± 181 km s^{-1} toward $l = 338$, $b = 10$, while the remainder of the sphere yields a mean flow of

TABLE 3

MEAN VELOCITIES AND ANISOTROPIES

R_e (km s^{-1}) Distance Range (1)	$(V_\odot - V_E)_x \pm \delta V_x$ $(V_\odot - V_E)_y \pm \delta V_y$ $(V_\odot - V_E)_z \pm \delta V_z$ (2)	$\lvert V_\odot - V_E \rvert \pm \delta V$ $l \pm \delta l$ $b \pm \delta b$ (3)	$\lvert V_{LG} - V_E \rvert \pm \delta V$ $l \pm \delta l$ $b \pm \delta b$ (4)	$h_1 + \delta h_1$ l_1 b_1 (5)	$h_2 + \delta h_2$ l_2 b_2 (6)	$h_3 + \delta h_3$ l_3 b_3 (7)
Bulk Flow Solutions						
≤3200	−375 ± 118	481 ± 106	419 ± 110	0.815 ± 0.056	1.060 ± 0.069	1.249 ± 0.061
	244 ± 93	147 ± 14	189 ± 14	213	254	336
	177 ± 75	22 ± 8	25 ± 11	59	−24	18
3200–8000	−207 ± 180	375 ± 172	544 ± 184	0.923 ± 0.053	0.973 ± 0.043	1.044 ± 0.048
	−110 ± 221	208 ± 43	243 ± 22	134	65	15
	292 ± 134	51 ± 24	33 ± 20	28	−35	42
≤8000	**−322 ± 102**	**420 ± 90**	**406 ± 91**	**0.906 ± 0.032**	**1.030 ± 0.048**	**1.100 ± 0.035**
	170 ± 84	**152 ± 15**	**202 ± 13**	**203**	**271**	**351**
	210 ± 65	**30 ± 8**	**31 ± 11**	**53**	**−16**	**32**
Solution with a Mass Concentration and no Bulk Flow						
≤8300	**−13**	**377**	**614**	**0.931 ± 0.033**	**0.992 ± 0.027**	**1.101 ± 0.040**
	−242	**267**	**269**	**324**	**271**	**206**
	289	**50**	**28**	**−39**	**37**	**−30**

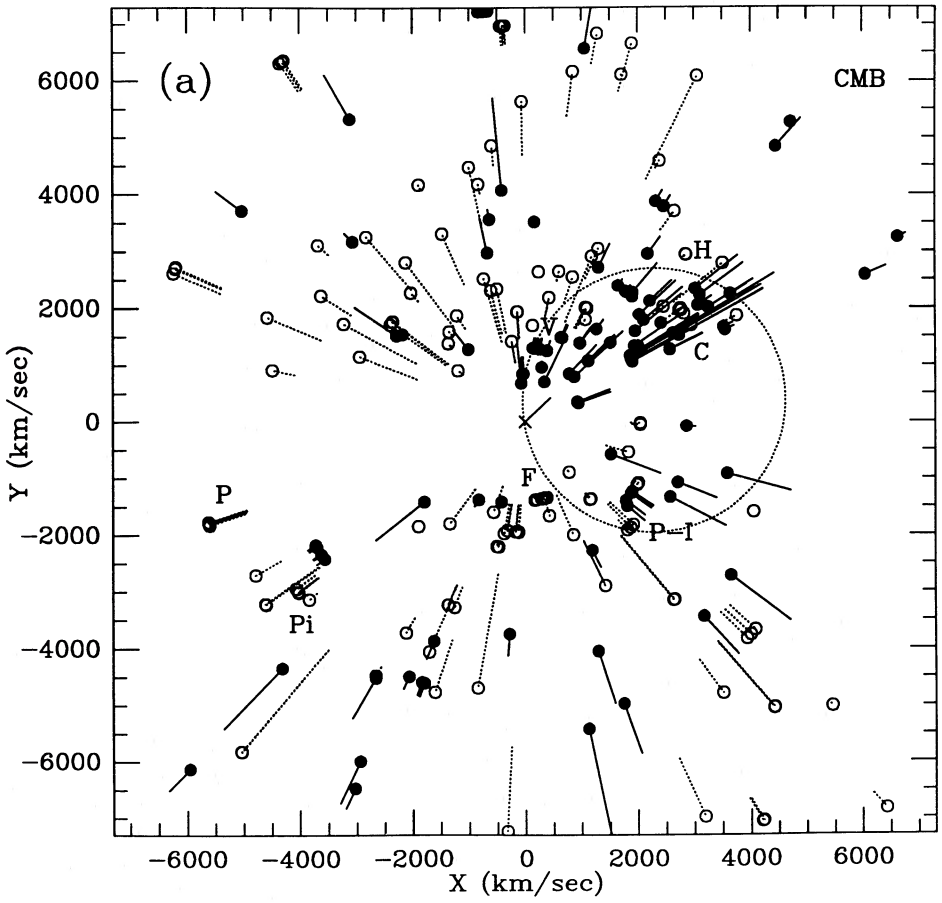

FIG. 6*a*

FIG. 6.—Peculiar radial velocity vectors for all objects within 45° of the supergalactic plane: (*a*) In the rest-frame. A massive concentration at $R = 4350$, $l = 307$, $b = 9$ would produce positive radial velocity residuals within the sphere drawn. (*b*) In the frame defined by the Bulk motion 521 km s^{-1} to $l = 307$, $b = 9$. Concentric circles are at distances of 2000, 3200, and 6000 km s^{-1}. (*c*) Residual peculiar velocities after subtracting those generated by the massive concentration and Virgo.

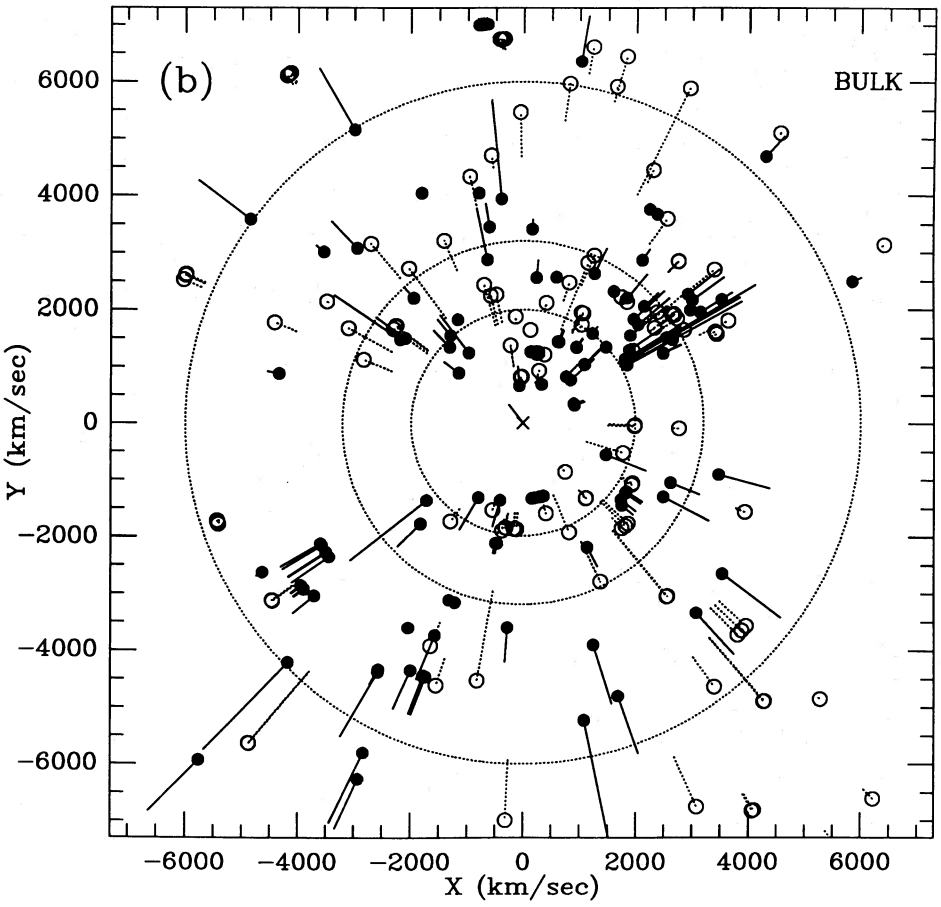

FIG. 6*b*

only 212 ± 107 toward $l = 246$, $b = 12$, a very different direction. Similarly, the backward directed 60° semiangle cone gives 632 ± 281 toward $l = 15$, $b = -6$. We conclude from these cone solutions that most of the mean motion seen in the all-sky solutions arises from within the cone pointed at (307, 9).

Figure 6*a* is a repeat of Figure 4*b* except that it shows all objects within 45° of the supergalactic plane rather than within 22°.5. The strong black lines on the right correspond to the clusters of ellipticals in Centaurus dominated by the NGC 4696 and NGC 4709 clusters. The NGC 4696 cluster has a heliocentric velocity of 3041 km s^{-1}, but a third of this is an excess velocity of ~1000 km s^{-1}. Probably in its background lies the NGC 4709 cluster. Its velocity is 4565, of which ~1500 km s^{-1} is excess over the Hubble flow. Thus, these Centaurus clusters are moving very fast. This contradicts the idea that it is the mass associated with them that is responsible for the observed streaming. Rather they are prime examples of rapidly streaming clusters.

However, the bulk streaming picture does not explain the Centaurus clusters' motion well. Even after the bulk motion is subtracted in Figure 6*b*, the Centaurus clusters still show prominent outward residual motion. By contrast, the Hydra and Antlia clusters some 25° away are almost at rest in the Hubble flow in the CMB frame and have inward residual motions in the frame of the bulk motion. However, they are too small in the wrong direction and at the wrong distance to be the mass that causes the streaming by themselves.

Finally, Figure 5*c* shows that evidence for streaming beyond $R_e = 3200$ km s^{-1} is relatively weak in our data—we have too few galaxies in the Centaurus directions beyond those we have just considered to say what happens there.

In summary, a uniform streaming motion over and above Hubble expansion in the CMB frame is certainly a better fit to the data than pure Hubble flow. However, it has serious defects:

1. It does not explain the curvature in Figure 5*b*, which shows that galaxies closest to the direction of the streaming show the greatest perturbation.
2. It does not explain the reduced slope in Figure 5*c*, which suggests that galaxies beyond 3200 km s^{-1} show less streaming motion.
3. It does not explain the quadrupoles and their alignment with the motion.
4. It leaves large residual motions in Centaurus and a large scatter, σ_f, about the mean flow; see Figure 6*b* and Table 2.
5. It does not explain the large changes in mean motion derived from different cones.

These shortcomings are circumvented by models with the streaming motion generated by a mass concentration. In the far field, such a concentration should generate a quadrupole in which the two short axes are of length $h_1 = 1 - V_m/R_m$ and the long axis points toward the flow and is of length $h_3 = 1 + 2V_m/R_m$, where R_m is the distance to the mass and V_m is the flow generated here. Taking $h_3 = 1.25 \pm 0.06$ and $V_m = 521$ km s^{-1} gives $R_m = 4200 \pm 1100$ km s^{-1}, but this distance is uncertain since the other two components of the quadrupole

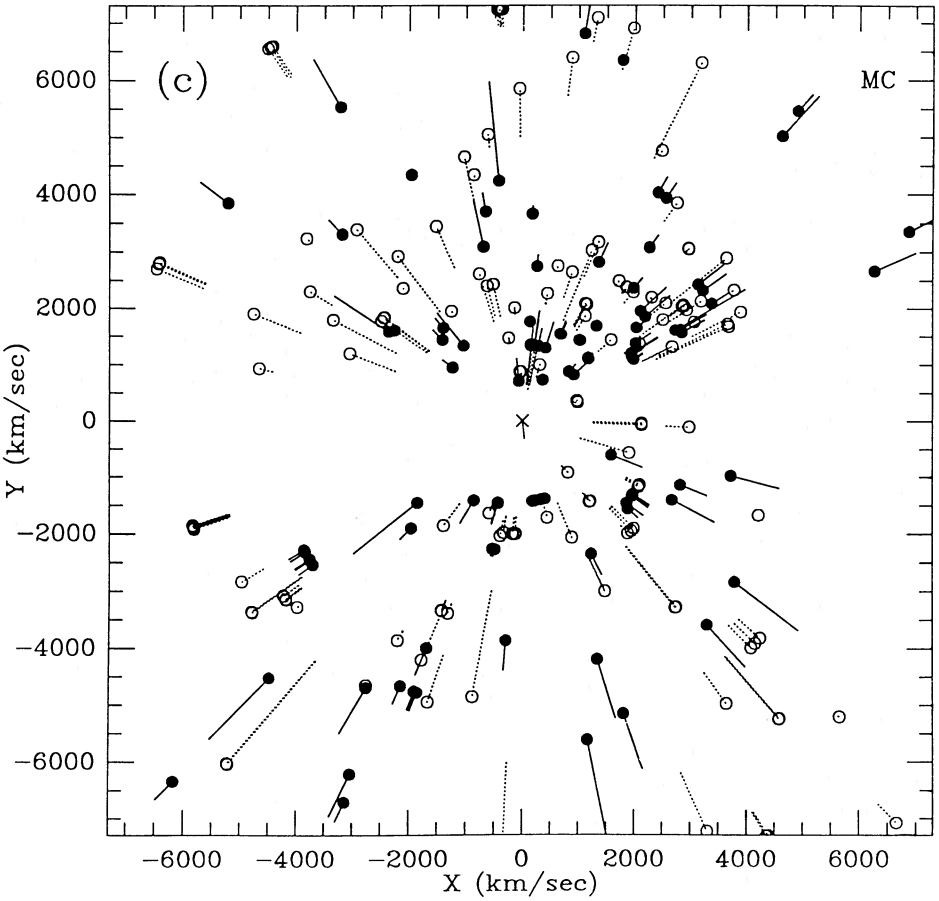

FIG. 6c

are unequal. We give more accurate estimates by detailed model fitting in the next section which allows for another mass concentration as well as that of Virgo.

b) *Flows Caused by a Mass Concentration*

It is natural to place the mass concentration in the direction of the observed flow $l = 307$, $b = 9$. There are then three extra parameters in our models: V_m, the velocity at the Local Group induced by the massive concentration; R_m, the distance to it in velocity units; and m, the power law by which the induced velocity falls with distance. After experiments we adopt $m = 1$, corresponding to a $1/r^2$ decrease in excess density away from the concentration. R_m and V_m are determined by maximizing the likelihood. The first solution (see lower part of Table 2) allows a bulk flow in addition to the mass concentration. It is much better than bulk-flow models in that the likelihood increases by 28 and χ^2 drops by 56. The former models gave improvements of only 15 and 30. Furthermore, the field velocity dispersion falls from 365 to 245, and the bulk flow drops to within 1.3 σ of zero. Thus, almost all the bulk motion has been accounted for by the gravity of the mass concentration, which induces 500 km s^{-1} at the Sun and is situated at a distance corresponding to 4200 km s^{-1}.

This success encouraged us to try solutions with the bulk flow set equal to zero. These are just as successful when the smaller number of parameters is accounted for. The best has a mass concentration that induces 570 ± 60 km s^{-1} at the Local Group, situated at a distance of 4350 ± 350 km s^{-1}, in good agreement with the quadrupole estimate above. This model is adopted as the standard mass concentration (MC) model and is shown in bold face. In these MC models we have maximized the likelihood by varying both σ_f and Δ. Since the spread of distance estimates to different objects within any one cluster is not used by the program, this double minimization provides a totally new estimate of Δ that is based on the distance dependence of $\sigma_e^2 = \sigma_f^2 + R^2(\exp \Delta^2 - 1)$. The values obtained by this method are $\Delta = 0.21 \pm 0.02$ and $\sigma_f = 250 \pm 40$, where the quoted errors allow for the correlation between Δ and σ_f which occurs because they both affect σ_e^2 in the same direction. The good agreement of this value of Δ with that from groups was noted earlier. The large value of σ_f obtained in the bulk-flow models has dropped most satisfactorily, demonstrating that this was due mainly to deficiencies in the model.

The remaining quadrupoles are still larger than one would like but the long axis may well be associated with another deviant region that is visible in Figure 4. This is the NGC 1600 and NGC 1700 region which has a large positive velocity residual of ~ 1000 km s^{-1} and lies toward $l = 200$, $b = -30$, close to the quadrupole direction (206, −30).

We have also investigated whether there is a significant improvement in the solution if the mass concentration is moved in direction from $l = 307$, $b = 9$. There is a slight improvement for positions a few degrees higher in b, but the likelihood change is small, and the difference is well within the errors quoted in Table 2.

VII. SOURCES OF ERROR

a) Random and Systematic Errors in the Data

Random distance errors can be gauged accurately from internal scatter in clusters and from the maximum-likelihood modeling errors. We have shown that both methods are consistent and indicate the streaming motion in the bulk model to be a 6 σ result. The MC model has even greater statistical significance. Random errors cannot conspire to cause the streaming.

The possibility of systematic errors in D_n has been investigated in several ways. The diameter D_n depends on the absolute photometric zero point and the absorption corrections. The sensitivity of log D_n to magnitude changes is given approximately by $\Delta \log D_n = 0.32\,\Delta B$. An apparent spurious motion of 900 km s^{-1} at 4000 km s^{-1} would thus require a systematic error in B of 0.35 mag. However, the discussion in Burstein *et al.* (1987) indicates that the photometric zero points in both hemispheres have been standardized to ± 0.03 mag, far smaller than the the required error.

Galactic absorption errors have been tested for in three ways:

1. We have redone the bulk-flow solutions using de Vaucouleurs's absorptions (de Vaucouleurs, de Vaucouleurs, and Corwin 1976) in place of Burstein and Heiles's. We have also redone the solutions using a cosec b law and also using no absorption corrections whatever.

2. We have omitted from the data set all objects whose estimated absorptions A_B are greater than 0.4 mag. This removes the three Centaurus clusters among others. The resultant bulk solution is given in Table 2, 470 ± 99 replaces 521 ± 89 km s^{-1}. None of these changes in the absorption treatment makes a very significant difference.

3. Finally, we have made an independent check on absorptions by using the fact that errors produce significant residuals in the Mg_2–$(B-V)$ relation. This relation is presented in Figure 7. Circles and stars denote galaxies toward the apex and antapex directions. The low straight line corresponds to the absorption error that would be needed to give a peculiar velocity of 900 km s^{-1} at 4000 km s^{-1}, which is typical of the apex galaxies in Centaurus. The high line corresponds to the observed 650 km s^{-1} peculiar motion of Perseus at 5800 km s^{-1}. Despite the fact that Centaurus and Perseus are both highly obscured regions, there is no sign of systematic absorption errors in either region of the magnitude required. This is consistent with the Mg_2 versus $(B-V)$ relation for the whole sample, which indicates that errors in the Burstein-Heiles reddenings for galaxies with $A_B \leq 0.6$ mag are less than 0.02 mag and show no systematic dependence on direction.

Systematic errors in σ are also too small to cause the apparent streaming. Errors of order $\pm 20\%$ are required, whereas Davies *et al.* (1987) show that the rms error is $\pm 10\%$, that the offsets between data sets from different telescopes average 3%, and that all are less than 6%. The conclusion is that random or systematic errors of measurement are all far too small to produce the measured streaming.

b) Residual Malmquist Errors

The Malmquist correction in equation (2.11) presumes that the sample of objects is uniformly distributed in space, whereas

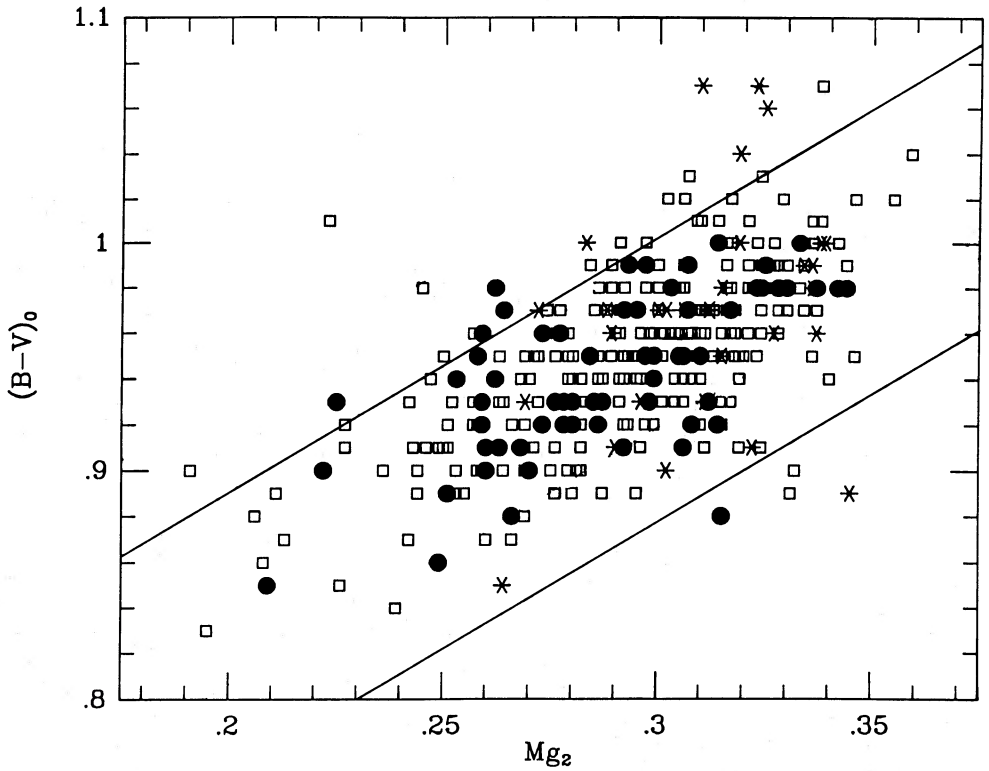

FIG. 7.—The Mg_2–$(B-V)_0$ relationship for 354 elliptical galaxies with measured motions. The 66 galaxies with cos $\vartheta \geq 0.75$ are denoted by closed circles, the 34 galaxies with cos $\vartheta \leq -0.75$ are denoted by stars, and the 254 galaxies in between these two directions are denoted by open squares. If absorption were to generate the apparent 900 km s^{-1} motion toward the apex, the closed circles should scatter about the lower line. If the 650 km s^{-1} motion of the Perseus region were due to absorption errors, the stars should scatter about the upper line. The agreement with the mean relationship shows that these motions are not due to misinterpreted absorption errors.

the actual space distribution of ellipticals is clumpy. Some of this clumpiness has been removed by assigning galaxies to groups, but significant large-scale gradients remain. This introduces distance errors into some of the model parameters; can it be the cause of the streaming motion? The main feature of the streaming is the large positive peculiar velocities of the galaxies toward Centaurus. If caused by a Malmquist effect, this would require the existence of a dense concentration of ellipticals just *at* or *beyond* the edge of the volume surveyed by the data. Such a concentration is implied by the MC model. Furthermore, we show in § VIII that available catalogs strongly indicate a major concentration in the right direction and at the right distance for the MC model. The crucial question for Malmquist errors is then two-fold: (1) does the mass concentration contain an excess of elliptical galaxies as well as spirals, and (2) what is the depth of the sample in this direction compared to the distance of the mass concentration? The second point is relevant because there should be no net Malmquist streaming if we see well beyond the concentration, and we should even expect to see galaxies falling in from the other side.

We initially believed that the sample must extend well beyond the mass concentration at 4350 km s^{-1} because it contains many ellipticals at greater distances in other directions (see Fig. 6). However, because we fail to see a major component of ellipticals there that is either stationary or falling in from the rear, the mass concentration itself and the regions on the backside would have to be severely deficient in ellipticals. This conclusion is sufficiently bizarre that it prompts us to seek an alternative explanation.

A second look at the galaxy catalogs from which the target sample was chosen suggests a possible answer. Galaxies towards Centaurus were selected from the southern ESO Catalog. A cursory check of Hubble types in this direction shows a significant excess of early Hubble types, not a dearth as required by the above hypothesis. However, there seems also to be a systematic error that misclassifies faint E's as S0's near $B = 13.0$ mag (our magnitude limit). Thus they are missed. We give a more quantitative discussion of this effect in Faber *et al.* (1988), but the net result is that the southern sample does not appear to be as deep as the northern one and has not penetrated as far as the mass concentration. Since there does seem to be a density excess just at or beyond the edge of the sample, there may indeed be a spurious Malmquist contribution to the large streaming velocities in Centaurus.

Estimating the size of this error requires a knowledge of the true space distribution of ellipticals along this line of sight, which is presently unknown. We can obtain some feeling for the sensitivity of the solution, however, by modifying the value of the space-density exponent α in equation (2.3). A cone solution for bulk streaming velocity with semi-angle 60° toward the apex direction in Centaurus yields 913 ± 181 km s^{-1}, as noted above in § VI*a*. This solution, like all others, assumes a uniform space distribution with $\alpha = 3$. We have rerun this solution with $\alpha = 4$ and 5 to simulate an increase in space density along the Centaurus line of sight. For each change in exponent of unity, the bulk streaming velocity goes down by 45 km s^{-1}. Thus, if the streaming would be reduced from 913 to 823 km s^{-1}, a change of this magnitude would not have a major impact on the parameters of the mass concentration model.

A more pertinent question is whether Malmquist errors are significantly inflating the estimated field velocity dispersion. Errors in radial velocities work in the same direction. For both these reasons, the quoted value $\sigma_f = 250$ km s^{-1} for the best-fitting MC model will be an overestimate. Nevertheless, from fitting similar spiral data to MC models, we think the difference between our field σ_f of 250 km s^{-1} for ellipticals and the value 150 km s^{-1} often quoted for spirals (AHMST 1986) is probably real.

c) *Systematic Variations in Galaxy Properties: Tests with a Simple Least-Squares Fitting Method*

Other observations can be combined to yield additional distance indicators, including D_n-Mg_2, L-σ, and L-Mg_2. We have tested these and also our model fitting method by using a simple least-squares program without any weights, Malmquist corrections, or group diameter-bias corrections. The results for bulk-flow models are shown in Table 4. The high bulk-flow velocities remain, but none of these other methods has the accuracy of the D_n-σ relation. Substitution of Mg_2, however, demonstrates that σ by itself is not a faulty parameter.

It can be shown that all of the above distance indicators including D_n-σ are based on the fundamental assumption that mass-to-light ratio is a well-behaved function of the basic structural variables for ellipticals. In Faber *et al.* (1987), it was shown that M/L_B varies as $L^{0.24\pm0.04}I_e^{0.00\pm0.06}$, where I_e is average surface brightness. Intrinsic scatter about this relation for cluster galaxies is only ±15%, but the data are insensitive to zero-point differences among clusters, which are indistinguishable from distance effects.

To explain the streaming motion this way, it would be necessary to assume that the M/L_B of ellipticals toward Centaurus is

TABLE 4

PURE LEAST-SQUARES SOLUTION WITH DIFFERENT DISTANCE INDICATORS[a]

Distance Indicator	v_{max} CMB Frame	$v_E - v_{CB}$ (km s^{-1})	l	b	N
$\sigma^{1.2}/D_n$	<9000	659	283	−14	344
$\sigma^{1.75}/I_B^{0.5}$	<9000	611	270	0	344
$Mg^{4.17}/D_n$	<9000	716	281	−10	344
$Mg^{5.24}/I_B^{0.5}$	<9000	826	262	−9	344
$\sigma^{1.2}/D_n$	<6000	524	299	9	263
$\sigma^{1.75}/I_B^{0.5}$	<6000	606	267	14	263
$Mg^{4.17}/D_n$	<6000	734	281	−2	263
$Mg^{5.24}/I_B^{0.5}$	<6000	765	265	−1	263

[a] All points are unweighted.

systematically 35% smaller than elsewhere. While this possibility cannot be ruled out, the residuals of Mg_2 on velocity dispersion, which one might expect to be sensitive to M/L variations, show no correlation with peculiar velocities. Moreover, the evidence on spiral galaxy motions studied by other workers and the space density of galaxies in Centaurus presented below strongly argue against this explanation. They suggest that the galaxy properties themselves are not the cause and that the motion is real.

The motion is *not* caused by deviant measurements in the Centaurus *clusters*. The three clusters there have $A_B \sim 0.5$ and are not included in the solution with $A_B < 0.4$, which yields a bulk flow of 470 ± 99 in place of 521 ± 89 km s^{-1}. A large region of the sky contributes, not just a few clusters.

VIII. THE SUPERGALAXY

a) Is the Mass Concentration Visible?

Since the identification of Hydra-Centaurus as a possible supercluster by Chincarini and Rood (1979), there has been much interest in whether it can be a significant influence on our motion relative to the CMB. Shaya (1984) and Tammann and Sandage (1985) showed that the Local Group's motion could be a compound of a Virgo infall plus a motion toward Hydra-Centaurus in which Virgo took part. However the situation became much more confused when we found the ellipticals that dominate the Centaurus double cluster to be moving even faster than the mean flow. It is essential from here on to distinguish these foreground Centaurus clusters from the massive concentration that causes the flow and which must lie beyond them.

We shall later rename this aggregate the "supergalactic center." We emphasize that its distance is at about $R = 4400$ km s^{-1} and that the Hydra-Centaurus supercluster originally identified by Chincarini and Rood between $2200 < V_0 < 3600$ km s^{-1} and followed up by Tammann and Sandage is in the foreground. However, the later work in this region (da Costa *et al.* 1986; Lucey, Currie, and Dickens 1986; Lucy 1986; Dickens, Currie, and Lucey 1986) has penetrated to the background at ~ 4300 km s^{-1}, which we identify with the supergalactic "bulge." It is interesting that Hopp and Materne (1985), working 30° away in the sky in the Hydra-Antlia region, still find a concentration of background redshifts at about this value.

To see the object concerned, we first looked on sky survey plates in the direction of our motion (307, 9). This is too close to the Galactic plane for serious studies of the extragalactic world. Cirrus contamination is a serious hazard in using the *IRAS* data in this region, and we were unable to find any obvious concentration of X-ray clusters in the *HEAO 1* map of the X-ray sky. However, we noticed the great concentration of galaxies in northern Centaurus at $\sim 13^h20^m$, $-29°$ in the ESO Survey (Lauberts 1982), and this is well represented in Lahav's quasi photograph given in Lynden-Bell (1986). To see this structure more clearly we decided to take new axes so that the direction of our motion $l = 307$, $b = 9$ lies in the center of the plot. Ofer Lahav then computed for us a new picture based on all the galaxies in the ESO, UGC catalogs plus those from the Morphological Catalog of Vorontsov-Velyaminov and Archipova (1963), where the former catalogs have a missing strip $-2 \leq \delta \leq -17.5$.

The resulting picture centered on the direction of our motion is Figure 8. It shows a complete hemisphere of the sky in an equal area projection. The dark vertical band slightly to right of center is caused by obscuration in the Galactic plane, but, in spite of this, the supergalaxy makes a most striking object. The Virgo, Centaurus, Hydra, and Antlia clusters are indicated. Looking at this picture and estimating the likely effect of absorption by eye, we estimate that the supergalactic center may lie at $l = 312$, $b = 18$, i.e., at supergalactic longitude of about $L = 162$, $B = 0$. This is within the errors of the direction of the bulk motion solution. However, we cannot yet exclude the possibility that the major supergalactic center lies at the concentration of what is already seen in northern Centaurus, around $l = 310$, $b = +29$.

Even without any help from more galaxies hidden behind the Galactic plane, this is a most remarkable concentration. We have compared the galaxy numbers in this region within a circle of 15° radius centered at $l = 310$, $b = +29$ with those in the 6° curcle around the Virgo cluster. These two radii correspond to roughly the same galaxy surface density. After allowing for absorption corrections to the number counts, we found that the galaxies in the ESO catalog in Centaurus with diameter $\geq 1'$ have true photoelectric diameter of $\geq 1'.21$. Since those galaxies are 3 times as far away as Virgo galaxies, we counted only galaxies that have true photoelectric diameters of $\geq 3'.63$ in Virgo. These correspond to Nilson diameters of $\geq 3'.30$. Moreover, from both sets of counts we must subtract suitable backgrounds taken from ordinary regions of the same area and at the same galactic latitudes. We cut at two diameter levels and compared not only galaxy numbers but also an approximation to their light, taking this to be proportional to the squares of their angular diameters. Four different estimates of the Centaurus/Virgo population ratio can then be found from Table 5. They are 16, 25, 17, and 29. Thus the visible concentration already has a population of the order of 20 times that of Virgo, even without allowance for anything hidden behind the Galactic plane or the extra galaxies in the extension seen along the supergalactic plane.

TABLE 5

GALAXY COUNTS IN CLUSTERS AND COMPARISON REGIONS[a]

MEASURE OF BRIGHTNESS	RADIUS = 15°				RADIUS = 6°			
	CENTAURUS		COMPARISON		VIRGO		COMPARISON	
	$\theta_{min} = 1$	$\theta_{min} = 1.3$	$\theta_{min} = 1$	$\theta_{min} = 1.3$	$\theta_{min} = 3.3$	$\theta_{min} = 4.3$	$\theta_{min} = 3.3$	$\theta_{min} = 4.3$
N	1391	690	370	156	70	35	7	4
$\Sigma\theta^2$	5957	5047	811	540	1982	1512	163	127

[a] Raw catalog diameters. These have been matched to correspond to a factor of 3 in relative distance, as explained in the text.

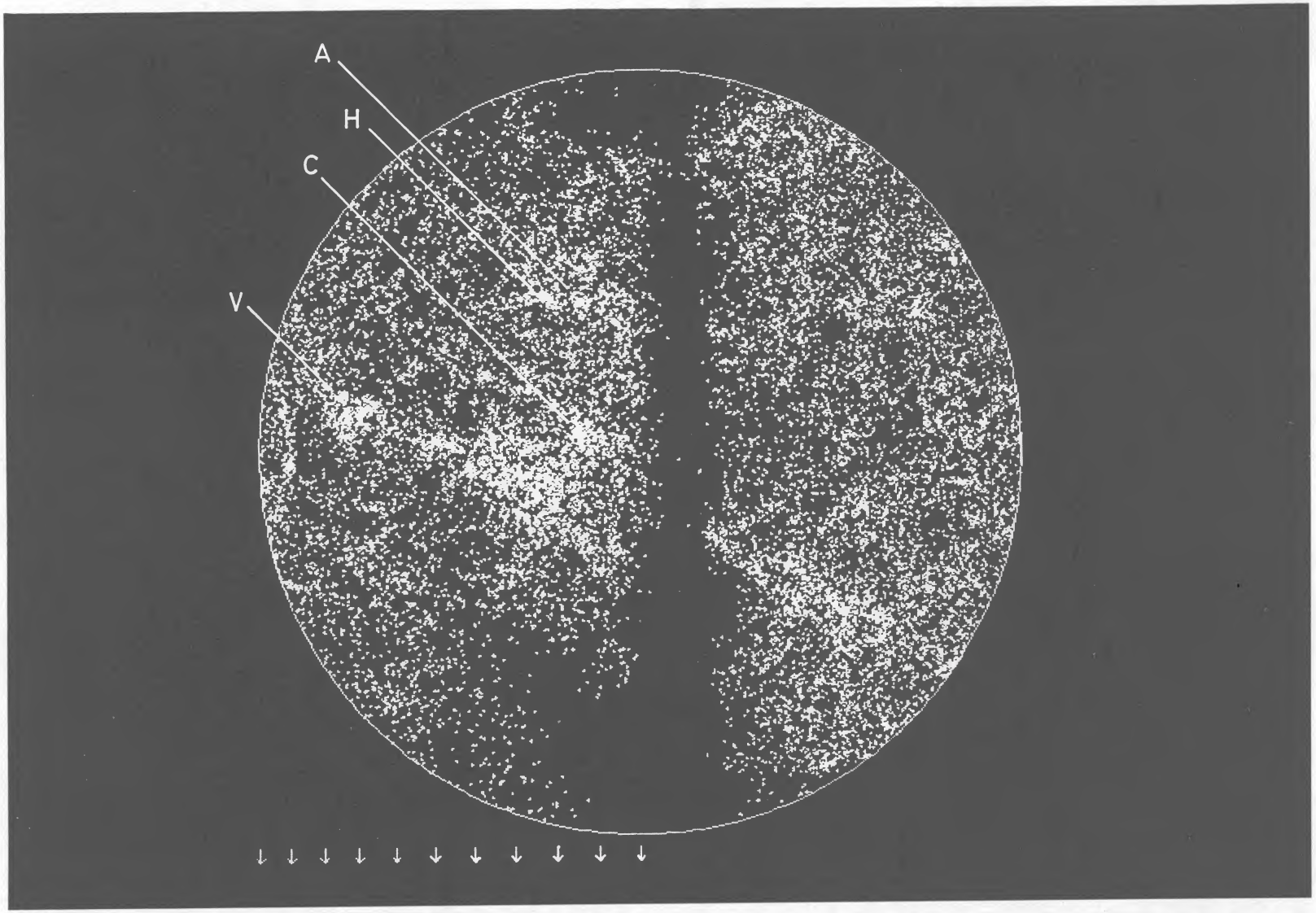

FIG. 8.—Computer plot of the supergalaxy made by Lahav from the ESO catalog of galaxies, supplemented by the UGC for the north and the Morphological Catalog for the $-2° > \delta > -17\overset{\circ}{.}5$. The picture is centered on the direction of the streaming, $l = 307$, $b = 9$, and contains a hemisphere of the sky in an equal area projection. The zone of avoidance caused by the Galaxy is the dark vertical band. The Galactic center lies 37° up from the bottom. The Virgo, Centaurus, Hydra, and Antlia clusters are indicated. The great concentration of galaxies just below the Centaurus cluster is obvious. The nonlinear scale indicates 9° radial intervals; those at the left are appropriate to the edge of the picture, those at the right are appropriate for the center.

b) Properties of the Supergalaxy

The major gravitating center in the supergalactic plane lies in Centaurus beyond the prominent clusters of ellipticals. This concentration is so great that even here it causes a greater infall than the Virgo Cluster, 570 km s^{-1} as opposed to $\sim$250 km s^{-1}. The supergalactic band of galaxies stretches from Centaurus through Virgo and on to Ursa Major, where it extends from the Local Group out to $\sim$2000 km s^{-1}. In the other direction, the supergalaxy extends from Centaurus through Pavo Indus as a prominent band on the sky. There we have evidence that it has some depth since objects in it have velocities as different as 2000 and 7000 km s^{-1}, yet apart from the bulge in Centaurus it is only 8° thick.

However, the simple view that the supergalaxy is like the Milky Way, but with each star replaced by a galaxy, does not explain all the observed facts. There seems to be a void with very few galaxies beyond the supergalactic center in Centaurus. The redshift surveys show almost nothing between 5500 and 8500 km s^{-1}. The supergalaxy, though apparently thin, is not rotating, and the visible portion of its "bulge" seems to contain no great elliptical clusters other than those in the foreground.

To estimate the excess mass in the supergalaxy over and above that which normally occupies such a volume, we use the formula $v\,\Delta v = G\,\delta M/r$, where v is the Hubble velocity, 4400 km s^{-1}, Δv is the peculiar velocity, 570 km s^{-1}, and r is the distance. We thus find

$$\delta M = 5.4 \times 10^{16}\ M_{\odot}\, h_{50}^{-1}\ .$$

Values only a factor 2 less than this were quoted by Tammann and Sandage in their search for the object that generated the velocity of the Local Group in the CMB frame. They were guided by the unexplained part of that velocity vector to look in Hydra, and they assumed the object to be somewhat closer, 3000 km s^{-1} rather than 4400.

The visible "bulge" is 1100 km s^{-1} or $22h_{50}$ Mpc in "radius," and the velocity dispersion there we can take from the data of da Costa *et al.* (1986) (see also Melnick and Moles 1987). Da Costa *et al.* conducted a redshift survey in this region and found a strong peak in the number of galaxies whose breath corresponds to a dispersion of 1052 km s^{-1}. The mean heliocentric velocity of this peak (all 72 galaxies with $2500 < v < 7000$) is 4355 ± 124. Transforming this to the CMB frame gives 4654 ± 124 km s^{-1} in good agreement with our totally independent estimate of 4350 ± 350 from the motions of ellipticals all around the sky. Crude comparisons to the masses, radii, and densities of regions surrounding rich Abell superclusters indicate a general similarity, although as yet we see no rich cluster of ellipticals occupying a central place in the supergalaxy. Moreover, estimates of peculiar motions of 1000–2000 km s^{-1} among Abell clusters have been made by Bahcall, Soneira, and Burgett (1986). While it is probable that the supergalaxy is similar in morphology to the clustering of Abell clusters, the apparent lack of a central rich cluster of ellipticals could be due either to obscuration by the disk of the Milky Way or to the center having not yet collapsed.

IX. COMPARISON WITH OTHER DATA

a) Other Galaxy Surveys

Table 6 compares our results for elliptical galaxies with results already published in the literature, reexpressed as a velocity of the Sun relative to an appropriate reference frame. This frame is defined either by the cosmic microwave radiation or by spiral galaxies or by elliptical galaxies. The entries are ordered by distance. The near-field results ($R_e \leq 3200$ km s^{-1}) show some consistency in that the x-component is quite strongly negative, the y-component near +200 km s^{-1}, and the z-component also near +200. Of greater significance are the mean velocities of the galaxies relative to the frame defined by the microwave background, shown in the right half of the table. Here the x-component is large and positive, the y-component over 400 km s^{-1} and negative, and the z-component around 100 km s^{-1} and positive. There is no evidence here for random scatter about zero. Rather, there is definite evidence that the mean of the galaxies moves relative to the microwave frame. (There is, however, a lack of agreement between this conclusion and that of Hart and Davies [1982]. The meaning of the latter conclusion will soon be clarified in the publication of a more extensive work by Staveley-Smith and Davies.)

In the far field beyond $R_e = 3200$ the agreement among investigators is not as good, but the measurements are also less accurate. The agreement between the elliptical galaxies and the CMB frame is good, and the agreement with the cluster survey of ABMHSC is quite satisfactory. This can be understood in terms of the spatial distribution of the two samples. The far-field ellipticals contain little or no contribution from galaxies close to the direction of motion, $l = 307$, $b = 9$. Likewise, the 11 clusters in the Arecibo ring of ABMHSC come no closer than roughly 60° to this direction. The streaming velocity falls with distance away from Centaurus. When one looks out away from the supercluster beyond a few thousand km s^{-1}, one evidently encounters a reference frame that is close to the CMB zero point.

This concurrence with both the CMB frame and the ABMHSC cluster result differs somewhat from our previous report in Dressler *et al.* (1987*a*). This change has occurred because we were previously analyzing in velocity shells, so the furthest and fastest moving Centaurus cluster at 4500 km s^{-1} always lay in our outer shell. Now we cut in distance and have chosen the cut to be at a distance (3200 km s^{-1}) just beyond that cluster (it has a peculiar radial velocity of $\sim$1500 km s^{-1}). With this choice our far-field sphere now avoids the Centaurus contribution and thus shows little motion.

This leaves the Rubin-Ford result, which disagrees with the CMB. Like the far-field ellipticals and the ABMHSC clusters, the Rubin-Ford spirals lie mainly away from the direction of motion and outside the volume of space presently modeled. The original Rubin-Ford results have recently been bolstered both by Peterson and Baumgart (1986) and by Collins, Joseph, and Robertson (1986). The Rubin-Ford sample has many galaxies in the Perseus-Pisces-Lynx volume of space, which Haynes and Giovanelli (1986) show to have their own large-scale motion. We plan to rediscuss the Rubin-Ford galaxies along with data from all sources in a later paper.

Figure 9 illustrates the agreement of different authors in the direction of galaxy streaming and also illustrates the direction of the Local Group's motion relative to the CMB. The directions of the streaming motions of spirals in that frame agree with one another and are close to both the direction of elliptical galaxy streaming and to the rapid expansion axes of the Hubble tensor determined from ellipticals Q_E and from spirals Q_3. Revision of Lahav's optical dipole (Lahav *et al.*, in preparation) takes the dipole, from the published direction shown, to $l = 265$, $b = 20$, very close to the Local Group's

TABLE 6

SOLAR MOTION SOLUTIONS FROM GALAXY SURVEYS[a]

REFERENCES	SAMPLE GALAXIES	SUN WITH RESPECT TO GALAXIES v_x δv_x	v_y δv_y	v_z δv_z	$\lvert v_\odot - v_g \rvert$ (l, b)	GALAXIES WITH RESPECT TO COSMIC BACKGROUND RADIATION v_x δv_x	v_y δv_y	v_z δv_z	$\lvert v_g - v_{CB} \rvert$ (l, b)	N
				Near Field, $\lesssim 3000$ km s^{-1}						
1	Spirals	−74	107	302	329	61	−349	−13	355	300
	IRTF	(70)	(70)	(40)	125, 67	(70)	(70)	(40)	280, −2	...
2	Spirals	−167	230	210	353	154	−472	79	502	270
	IRTF	(70)	(70)	(80)	126, 37	(70)	(70)	(80)	288, 9	...
3	Spirals	−193	166	178	310	180	−408	111	460	500
	Tertiary	(31)	(50)	(47)	149, 35	(31)	(50)	(47)	294, 14	...
4	E gals	−375	244	177	481	362	−486	112	616	179
	$R_e \leq 3200$	(118)	(93)	(75)	157, 22	(118)	(93)	(75)	307, 10	...
				Far Field, $\gtrsim 3000$ km s^{-1}						
4	E gals	−207	−110	292	374	194	−132	−3	235	193
	$3200 < R_e \leq 8000$	(221)	(180)	(134)	208, 51	(221)	(180)	(134)	326, −1	...
5	ScI	−420	420	−84	600	407	−662	373	862	96
	$3500 < R_e < 6500$	(150)	(150)	(150)	135, −8	(150)	(150)	(150)	302, 26	...
6	ScI	−601	519	124	804	588	−761	165	975	96
	$3500 < R_e < 6500$	(150)	(150)	(150)	139, 9	(150)	(150)	(150)	308, 10	...
7	Cluster spirals	−192	−417	241	518	179	175	48	254	164
	IRTF	(200)	(210)	(200)	245, 28	(200)	(200)	(200)	44, 11	...
Sun with respect to cosmic background		−13 (10)	−242 (10)	289 (10)	377 267, 50					

[a] Velocities are in km s^{-1}.

NOTES.—Our x, y, and z components are the (cos l cos b, sin l cos b, sin b) components along the directions toward the Galactic center, of Galactic rotation, and toward the north Galactic pole. AHMST's results were quoted in a coordinate system based on M87 so we have performed the necessary conversion to find their motion of the Sun relative to distant spirals. They allowed for their Virgo infall model and we have used their total motion of the Local Group and converted it back to a motion of the Sun.

De Vaucouleurs and Peters (1985) quote solar motion with respect to galaxies in various distance ranges. We have averaged their first five entries which are pretty consistent and include all their galaxies out to ~ 3000 km s^{-1}. The errors we quote are the errors in those averages. They did not employ a Virgo flow model, but our experience with our elliptical galaxies out to 3000 km s^{-1} is that the net average only moves by some 50 km s^{-1} when a Virgo infall is incorporated.

Of the several solutions quoted by Peterson and Baumgart (1986) we have used the restricted Schecter solution. It is in good accord both with the original Rubin *et al.* (1976*b*) result and with Schechter's re-reduction of it.

REFERENCES.—(1) AHMST; (2) Lilje, Yahil, and Jones 1986; (3) de Vaucouleurs and Peters 1985; (4) This paper; (5) Rubin *et al.* 1976*b*; (6) Peterson and Baumgart 1986; (7) ABMHSC.

motion. A new selection of *IRAS* sources by color gives similar agreement, $l = 273$, $b = 31$ (Harmon, Lahav, and Meurs 1987).

There is a deviation between the streaming direction and those defined by the Local Group's motion and the dipoles. This is not totally unexpected. The large-scale motions do not include a contribution from Virgo infall, nor from such other local fields that affect the Local Group's motion. Any difference may well be sought among the brightest 300 galaxies rather than on the grand scale.

b) *The Local Group's Motion*

If we add the velocity generated by the Virgo cluster to the motion of 570 km s^{-1} toward $l = 307$, $b = 9$ generated by the mass concentration, we might hope to explain the Local Group's motion in the CMB frame. Unfortunately this hope is not fulfilled. In fact we find

supercluster: 570(307, 9) = (339, −449, 89),

Virgo (from AHMST): 250(284, 75) = (16, −63, 241),

Sum = (355, −512, 330),

The Local Group's motion is (−13, −542, 289). This leaves a part of the Local Group's motion unexplained (−368, −30, −41).

Since the distant shell of our elliptical galaxies agrees with the microwave frame, the objects that cause the above motion should be well within the region studied. Furthermore, the x-component of the bulk flow for the solution 0–2000 agrees quite closely with the local infall velocity toward the mass concentration. Thus it seems likely that the Local Group's peculiar motion is generated well within this smaller volume. It is perhaps worth remarking that $\sim 50\%$ of the optical dipole found by Lehav comes from the 500 largest galaxies, so a similar fraction of the gravity and velocity at the Local Group may be generated within the Virgo flow region. We leave this intriguing problem to the more detailed studies that can be made from the spiral galaxies which sample the local flow more densely.

X. COSMOLOGICAL IMPLICATIONS

a) *Dynamical Constraint on* $\delta\rho/\rho$ *and* Ω_0

For given Ω_0, the size of the density perturbation $\delta\rho/\rho$ required to induce the observed supercluster inflow is given by (Peebles 1980)

$$\Delta v = \tfrac{1}{3} H r \Omega_0^{0.6} \, \delta\rho/\rho \, . \qquad (10.1)$$

Taking $\Delta v = 570$ km s^{-1} and $Hr = 4400$ km s^{-1}, we find the

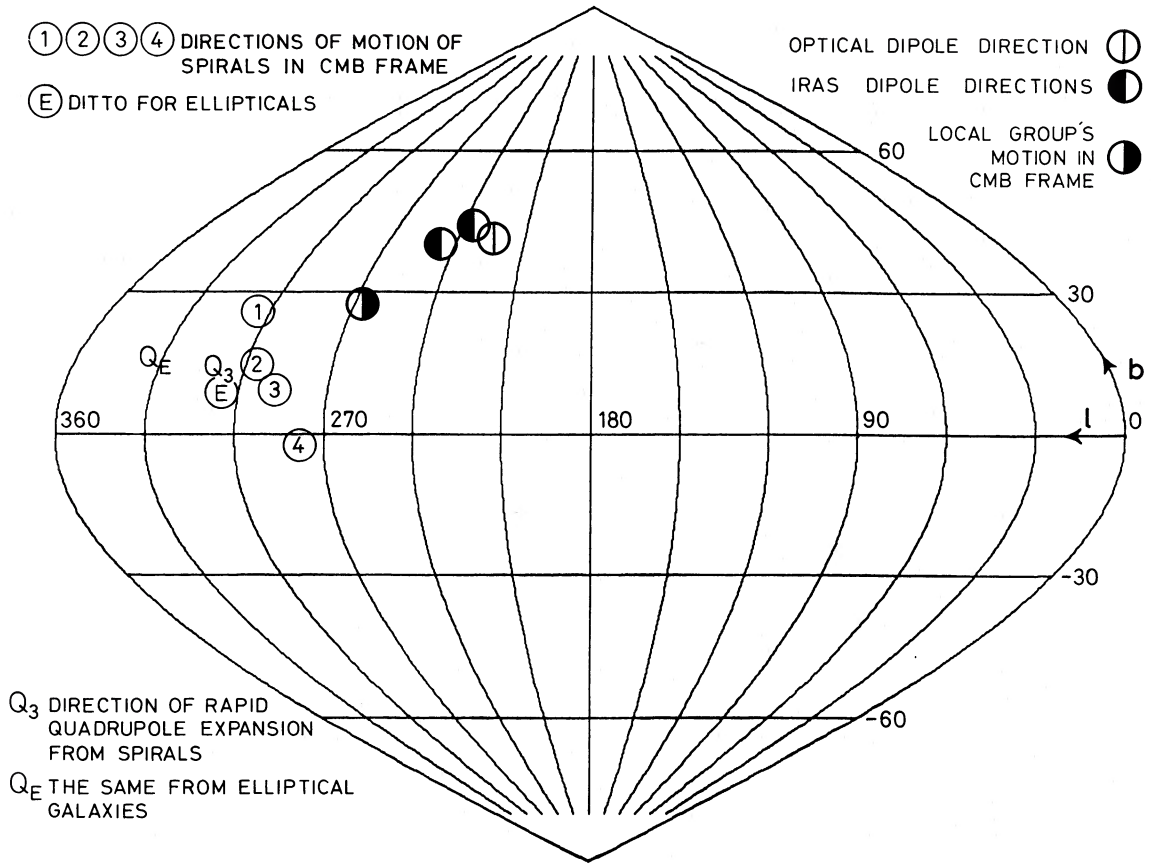

FIG. 9.—Chart of interesting directions in Galactic coordinates. All mean motions are in the CMB frame. Circled numbers indicate the following: (1) Mean motion of Rubin-Ford spirals, 862 km s^{-1}. Peterson and Baumgart's revision brings this direction into coincidence with the data indicated by a circled "E," but increased the velocity to 976 km s^{-1}. (2) Mean motion of de Vaucouleurs and Peter's spirals, 460 km s^{-1}. (3) Mean motion of AHM spirals according to Lilje, Yahil, and Jones (1986), 502 km s^{-1}. (4) Mean motion of AHMST spirals, 355 km s^{-1}. A circled "E" indicates that the mean motion of ellipticals with $R_e < 8000$ km s^{-1} is 521 ± 89 km s^{-1}. Q_E indicates the direction of the rapid expansion eigenvector of Hubble tensor determined from elliptical galaxy motions, 1.25 ± 0.06. Q_3 is the same as Q_E, but determined from spirals by Lilje, Yahil, and Jones (1986), 1.15 ± 0.04. A half-filled circle, dark on the right, gives the direction of the mean motion of Local Group 614 ± 27 km s^{-1} (Lubin *et al.* 1985; Fixen *et al.* 1983). A half-filled circle, dark on the left, indicates directions toward *IRAS* infrared flux dipole according to Meiksen and Davis (1986) and Yahil *et al.* (1986). A divided circle indicates direction toward optical flux dipole of Lahav (1987). Latest determinations place both optical and *IRAS* dipoles much closer to the Local Group motion (*see text*).

cosmologically interesting result

$$\Omega_0^{0.6}\,\delta\rho/\rho = 0.37\ .$$

For $\Omega_0 = 1.0(0.2)$, this gives $\delta\rho/\rho = 0.40(1.05)$.

The galaxy counts in the ESO and Nilson catalogs have a depth that is slightly greater than the radius of the supercluster and show fluctuations of order $\frac{1}{3}$ in surface density on scales of order a hemisphere. Thus neither of the above numbers appears impossible from present data.

Much more complete redshift surveys will be needed in the southern supergalactic plane before $\delta\rho/\rho$ is well constrained. Furthermore, the accuracy of equation (10.1) in practical application has been questioned by Bushouse *et al.* (1985) and Villumsen and Davis (1986).

b) Microwave Background Anisotropy

Additional cosmological constraints arise from consideration of the isotropy of the microwave background, provided that the last scattering surface was close to recombination at $z \sim 1000$. At this time the horizon size was of order 10,000 km s^{-1} in comoving coordinates, i.e., not much larger than the radius of the supercluster as found from our data. Fluctuations in gravitational potential on this scale would have led to fluctuations in the microwave background of order $\Delta T/T \approx -\frac{1}{3}\psi/c^2$ over scales of $\sim 1°\Omega_0$.

For spherical perturbations, the Sachs-Wolf formula leads to temperature variations

$$\frac{\Delta T}{T} = \frac{1}{2}\left(\frac{2}{5}\,\Omega_0^{-1/2} + \frac{2}{5} + \frac{1}{5}\,\Omega_0^{1/2}\right)\int_0^{\infty}\left(\frac{V}{R}\right)\Delta v\, dR/c^2\ , \quad (10.2)$$

where the integral extends from the center of the perturbation, $V(R)$ is unperturbed velocity, $\Delta v(R)$ is the velocity perturbation, and all quantities correspond to the present epoch. Substituting the standard MC model with $\Delta v = 570(R/4300)^{-1}$ and using integration limits $R_u = 10R_l$ yields $\Delta T/T$ 3×10^{-5} for $\Omega_0 = 1$ and 4.5×10^{-5} for $\Omega_0 = 0.2$.

Doppler perturbations corresponding to 570 km s^{-1} can be estimated from equation (10.1). They are comparable to Sachs-Wolf if $\Omega_0 = 1$, but are well over 10^{-4} if $\Omega_0 = 0.2$. Doppler perturbations for the inner part of the supercluster would be a factor of 2–3 times larger still. An object as large as the whole supergalaxy would produce measurable fluctuations in the microwave background at the level of 10^{-4} if Ω_0 were as small as 0.2.

c) The Cosmic Energy Equation

The Layzer-Irvine cosmic energy equation (e.g., Layzer 1963; Fall 1975; Davis and Peebles 1977) relates the mean kinetic energy of a typical galaxy to a potential energy integral, J_2, over the galaxy autocorrelation function. The result is a relation between Ω_0 and the rms of one component of velocity, $\bar{v}$, of a typical particle with respect to cosmic rest (Davis and Peebles 1984):

$$\Omega_0 = [\bar{v}/(660 \text{ km s}^{-1})]^{-2} . \quad (10.3)$$

The present elliptical sample provides the first data that come close to producing a meaningful value of $\bar{v}$, but even so the problems of interpretation are severe. With large-scale flows over several thousands of km s^{-1}, it is essential to have a sample that covers a large volume of space. Our sample does this, and, in addition, its errors of measurement are well understood. However, ellipticals inhabit systematically dense regions, and hence their random velocities are probably higher than typical. It is not known whether this sample's volume is large enough to determine a fair mean.

The first number we have estimated is the rms dispersion of a typical elliptical galaxy with respect to the CMB, averaged over the whole sample. We obtain values in the range 500–590 km s^{-1}, with bigger values corresponding to bigger distance ranges sampled. The increase reflects the fact that large, high-σ clusters are rare and thus tend to lie at the edge of the volume. The above dispersion and the others given below have been corrected statistically for measurement errors in R and have been weighted accordingly (this means that nearby galaxies tend to have higher weight). However, no correction has been made for errors in the measured radial velocities or for residual Malmquist errors in R.

A second number of interest is the rms dispersion of field galaxies not assigned to clusters. This is 450–550 km s^{-1}, somewhat lower than the value above since the component due to cluster dispersions is now excluded. The uncertainty range quoted corresponds to Δ varying between 0.19 and 0.23, the maximum plausible range. Finally, we have the rms dispersion of group barycenters. The mean group radial velocities were derived from the mean of all measured group members, not just the ellipticals in the sample. The rms group dispersion is 400–450 km s^{-1}, again for the same range in Δ.

Comparing these three numbers we see that the groups are moving most slowly, followed by the individual field galaxies, with the typical individual galaxy moving the fastest. It is intuitively plausible that matter averaged on larger length scales should move more slowly. However, the difference in magnitude between the motions of groups and those of individual galaxies is not large. This suggests that the bulk of the kinetic energy of typical ellipticals is induced by density inhomogeneities on fairly long length scales, larger than those of individual clusters. This is consistent with our discovery of the large-scale inflow toward Centaurus. It further suggests that the rms motions of spirals will be lower, but not enormously lower, than those of ellipticals found here.

None of the above dispersions are as large as the 660 km s^{-1} needed for $\Omega_0 = 1$. Also, they are all upper limits; the first one in particular provides a firm upper limit to the cosmic velocity dispersion averaged over all galaxies. We conclude that $\Omega_0 = 1$ requires either (1) a negative contribution to J_2 on large scales not taken into account in equation (10.3) or (2) that galaxies are more highly clustered than the mass so that J_2 overestimates the potential energy. Both possibilities are plausible so reliable estimates of Ω_0 from equation (10.3) are not yet possible.

d) Comparison to a Specific Model: Cold Dark Matter

Using the calculations of Blumenthal (unpublished) and of Bond and Efstathiou (quoted by Bond 1987), the probability of occurrence in the cold dark matter model can be estimated for some of the significant velocity flows in the present observations. There is good evidence that the velocity perturbation fills each region, so the top-hat model is preferred. The biasing parameter b^2 gives the ratio of overdensity of galaxies to that of dark matter; $b = 1$ and 2 are considered.

The results are given in Table 7. We calculate the χ^2 and probability of occurrence of each event singly and also take into account crudely the fact that there are multiple volumes in the survey where each event might have occurred. The calculations assume $H = 50$ and $\Omega_0 = 1$, but the sensitivity to these parameters is not large.

The conclusion from the table is that $b = 1$ is generally consistent with the data, but that values of $b \geq 2$ seem highly improbable. Values of $b \geq 2$ are preferred in matching CDM to large-scale structure (e.g., White *et al.* 1987). The main evidence against this is the large-scale inflow speed in the supergalaxy. The major uncertainty in this conclusion is whether or not the present survey covers a sufficiently large volume to be

TABLE 7

PROBABILITY OF PECULIAR VELOCITIES IN COLD DARK MATTER MODEL[a]

Region (1)	Radius (km s^{-1}) (2)	Δv (3)	b (4)	σ_{pred} (5)	χ^2 (6)	P_1 (7)	P_2 (8)
NGC 1600–1700	~500	865 ± 129	1	730	3.85	0.28	1.00
			2	365	12.26	6×10^{-3}	1.00
Sphere around Local Group	2000	450 ± 50	1	440	3.02	0.39	1.00
			2	220	11.94	7×10^{-3}	0.11
Sphere toward Supergalactic center	~2000	913 ± 181[b]	1	440	8.57	0.035	0.43
			2	220	17.05	7×10^{-4}	0.011

[a] Meaning of columns: column (3), Δv, observed peculiar velocity of region *w/r* CMB; column (4), b, biasing parameter; column (5), σ_{pred}, rms three-dimensional velocity predicted by cold dark matter for $H = 50, \Omega_0 = 1.00$ (for sources see text); column (6), χ^2, chi-squared; column (7), P_1, probability of chance occurrence of Δv for a single event based on χ^2 and 3 degrees of freedom; column (8), P_2, probability of at least one occurrence of Δv in volume sampled; this is computed assuming total volume sampled is 5000 km s^{-1} in radius and there are N independent samples, where $N = (5000/\text{radius})^3$.

[b] Value is actually taken from bulk flow solution for 60° cone (semiangle) centered on direction 307°, +09°; see text for discussion.

random or is still strongly biased to the Local Supercluster. If so, the random probabilities of the CDM estimates might not apply.

Yet another way to compare with CDM is to evaluate the probability of occurrence of the overdensity $\delta\rho/\rho$ implied by equation (10.1) for the sphere centered on the supercluster inside the radius of the Local Group. With a radius of 4400 km s^{-1}, this sphere is 166 times more massive than the scale length on which the galaxy correlation function equals unity (800 km s^{-1}; Davis and Peebles 1984). From the graph of $\delta\rho/\rho$ versus M for cold dark matter given by Blumenthal *et al.* (1984), we find that the expected rms $\delta\rho/\rho$ on the mass scale of the supercluster is only $0.13b^{-1}\Omega_0^{-1/3}$, where b is the biasing parameter. This result is independent of H.

In § XI*a* we saw that $\delta\rho/\rho$ values ranging from 0.40 to 1.05 are required to produce the Local Supercluster inflow velocity. Although such estimates may have substantial error (Bushouse *et al.* 1985; Villumsen and Davis 1986), nevertheless both values are (3–5)b times larger than the CDM result. Taking into account the substantial uncertainties, we conclude once again that cold dark matter may be able to match the inflow velocity provided $b = 1$, but that $b = 2$ is essentially ruled out.

This conclusion differs from recent work by Bardeen, Bond, and Efstathiou (1987) and by Vittorio, Juszkiewicz, and Davis (1986) in that biasing values near $b = 1$ appears somewhat more favorable here. This is due in part to a slight reduction in the flow velocity in the present paper and in part to a more detailed treatment of the observational errors and probabilities. However, the major conclusion still stands that the favored bias values of $b \geq 2$ are in deep trouble.

Many people and organizations have helped this project. We particularly thank Ofer Lahav for making Figure 8 and the Centaurus richness calculation from the catalogs. J. Huchra kindly reran for us his group forming algorithms. Among others, C. Dalle Ore, J. Gonzalez, R. Jedrzejewski, R. M. Lynden-Bell, R. McMahan, R. P. S. Stone, Roy White, and R. V. Willstrop have helped in computing or observing while M. W. and C. Feast are especially thanked for their hospitality in Cape Town. We are grateful for the unstinting support of the staffs of Lick Observatory, SAAO, Anglo Australian Observatory, Palomar, Las Campanas, Kitt Peak, and Cerro Tololo. This work was supported by grants from NSF (AST82-11551), NATO, Arizona State University, University of Califoria at Santa Cruz, and the Royal Greenwich Observatory, Herstmonceux.

APPENDIX A

COSMOLOGICAL CORRECTIONS

For cosmological distance estimates, galaxy diameters are required that are measured to the same fixed point within a galaxy independent of its distance or velocity. Since D_n encloses a specified mean surface brightness, this need is accomplished once surface brightness is properly corrected for interstellar absorption and cosmological effects. The basic cosmological formulae used here may be found in Peebles (1971) and Weinberg (1972).

It is convenient to introduce three measures of distance. The first is

$$d_P = \text{proper distance} = R(t_0)r_1 , \tag{A1}$$

where r_1 is the dimensionless comoving coordinate distance and $R(t_0)$ is the present scale factor for the universe (the notation is Weinberg's). The second is

$$d_L = \text{luminosity distance} = \left(\frac{L}{4\pi l}\right)^{0.5} . \tag{A2}$$

where L is intrinsic bolometric luminosity and l is apparent bolometric flux density. The third is

$$d_S = \text{diameter distance} = \frac{S}{D} , \tag{A3}$$

where S is an absolute linear diameter and D is the corresponding angular diameter.

Weinberg shows that these three distances are related as follows:

$$d_L = d_P(1 + z) , \qquad d_S = d_P(1 + z)^{-1} , \qquad \text{and} \qquad d_S = d_L(1 + z)^{-2} , \tag{A4}$$

where z is the unperturbed Hubble redshift. Equations (A4) strictly apply only to a smoothly expanding universe with zero peculiar velocities. This is because there are factors in the bolometric fluxes that depend on transverse motion and actual redshift in addition to unperturbed redshift. However, we ignore these complications since the differences are small and the transverse motions are unknown.

Equations (A1) and (A3) and the fact that apparent surface brightness varies as $1/D^2$ yield the familiar law for bolometric surface brightness as affected by the expansion of the universe,

$$SB = SB_0(1 + z)^{-4} . \tag{A5}$$

The quantity D_n is therefore derived from the raw aperture magnitudes as follows: a correction is first applied for interstellar absorption (Burstein and Heiles 1982) and then the usual K-correction, which transforms the fluxes to equivalent bolometric fluxes (Humason, Mayall, and Sandage 1956). At this point equation (A5) applies. Multiplication of each aperture magnitude by $(1 + z)^4$ then yields the intrinsic rest-frame surface brightness, and thus D_n.

To predict a redshift from D_n, it is convenient to use an approximation for d_L at low z given by Weinberg:

$$d_L = (c/H)[z + 0.5(1 - q_0)z^2] . \quad \text{(A6)}$$

The error in this expression is only one part in 10^{-5}, or 3 km s^{-1}, at 9000 km s^{-1}. Equation (A4) then gives

$$d_S = (c/H)(1 + z)^{-2}[z + 0.5(1 - q_0)z^2] . \quad \text{(A7)}$$

Let us introduce the "naive redshift," $z' = (Hd_S/c)$. This is the redshift we would predict from the apparent diameter ignoring cosmological effects. Inverting equation (A7) and saving terms to second order yields

$$z = z'(1 + z')^2 - 0.5(1 - q_0)(z')^2 , \quad \text{(A8)}$$

which for $q_0 = \frac{1}{2}$ is simply

$$z = z'(1 + 7/4z') . \quad \text{(A9)}$$

The error in this expression at 9000 km s^{-1} is only 6 km s^{-1}. The first-order correction term amounts to 478 km s^{-1} at the same distance and is just significant. We have used estimated distance for z' in the term in brackets. Since our standard unit of distance is the distance to the Coma cluster, the correction actually applied is $\{1 + 7/4[z - z(\text{Coma})]\}$.

(It is interesting that the analogous correction term for redshifts deduced from apparent magnitudes is only $1 - 1/4z'$. Since this is some 7 times smaller than the correction term in equation (A9), naive luminosity redshifts would not require any correction over the distance range studied here.)

APPENDIX B

SLOPE AND ZERO POINT OF THE σ-D_n RELATIONSHIP: DIAMETER-BIAS CORRECTION FOR GROUPS

In establishing the slope and zero point of the σ-D_n relation a problem arises immediately: What coefficients should be considered "best"? It turns out that there is no really rigorous answer. Consider a field galaxy and a cluster at different distances and imagine that we are trying to measure the distance to the galaxy in units of the cluster distance. The situation is sketched in Figure 10. The best distance estimate corresponds to that shift which places the galaxy at the peak of the cluster probability distribution, $p(D_n \mid \sigma)$.

A fully rigorous approach to finding this peak would employ a maximum-likelihood technique that modeled the two-dimensional distribution function $p(\sigma, D_n)$. Instead we assumed that the locus of the peaks at different sigmas can be approximated by a linear

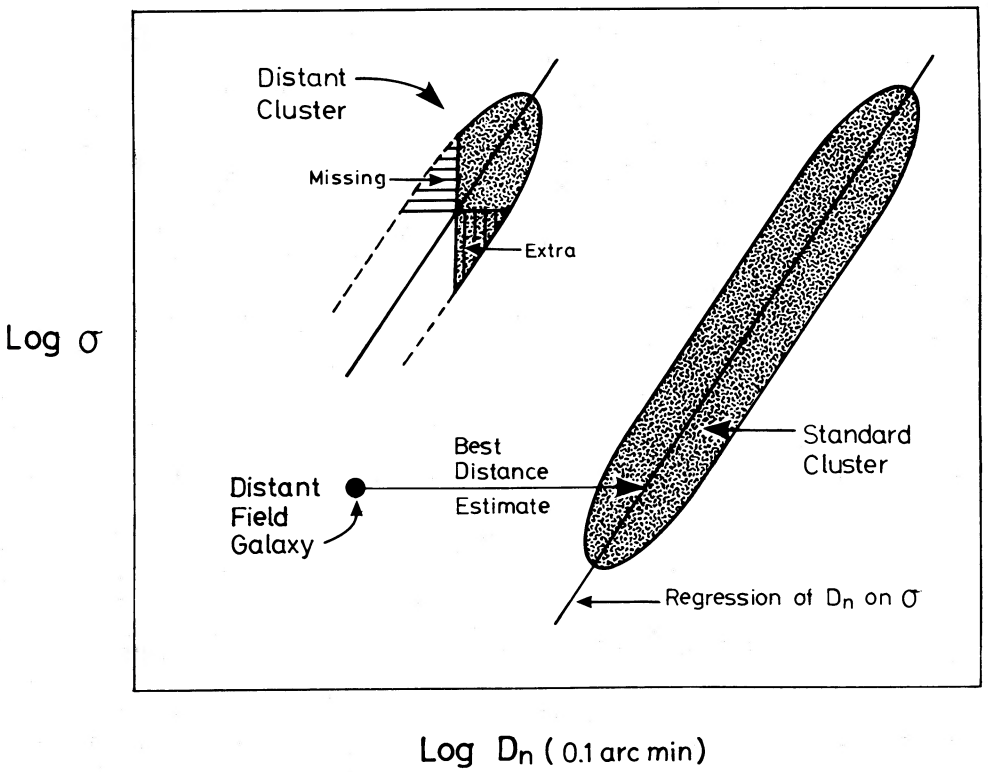

FIG. 10.—Diagram illustrating the distance estimators bias for cluster distances. The right shaded area represents the σ-D_n relationship for a standard cluster. The distance estimate log R_e for a field galaxy is given by the length of the horizontal arrow. In the upper left lies a more distant cluster that is not deeply sampled. The mean (and median) distance estimate for this cluster is biased too low because too many large galaxies are included above the D_n cutoff ("extra"), while galaxies that should be there are not ("missing").

TABLE 8

SLOPE OF THE D_n-σ RELATION FROM CLUSTERS

Group	log σ_{cut}	No. Galaxies	x	Δ
Virgo[a]	2.00	16	1.37 ± 0.12	0.082
	2.20	11	1.07 ± 0.26	0.080
Perseus	2.00	18	1.56 ± 0.28	0.120
Coma	2.00	33	1.24 ± 0.11	0.071
	2.20	27	1.46 ± 0.17	0.070
Pisces	2.00	7	1.02 ± 0.12	0.034
Fornax	2.00	11	1.16 ± 0.27	0.103
Centaurus	2.00	9	1.42 ± 0.29	0.085
Abell 2199	2.00	12	0.88 ± 0.41	0.140
DC 2345−28	2.00	10	0.88 ± 0.36	0.175
Eridanus	2.00	5	1.02 ± 0.29	0.079
Abell 194	2.00	6	0.83 ± 0.25	0.091
All (weighted mean)	2.00	127	1.21 ± 0.09	0.102
All minus Per, DC, A2199	2.00	87	1.19 ± 0.08	0.078
All (weighted mean)	2.20	96	1.17 ± 0.12	0.096
All minus Per, DC, A2199	2.20	64	1.20 ± 0.12	0.082

[a] Galaxy NGC 4486B is omitted.

relation with the same slope and zero point for all objects. This assumption gives the distance indicator defined in equation (2.1). We also assume that the residuals in log D_n are Gaussian distributed with dispersion Δ independent of σ. These assumptions allow us to ignore the two-dimensional distribution $p(\sigma, D_n)$ in favor of the conditional distribution $p(D_n \mid \sigma)$.

The "best" slope and zero point are those that yield the line that most closely approximates the locus of such peaks. If a least-squares fitting procedure is used to find this line, the regression of D_n on σ is needed. Ten of our groups and clusters contain enough galaxies to give reasonable fits. The individual least-squares fits and the scatter in log D_n for each cluster are given in Table 8. Since D_n is being fitted on σ, we should choose clusters free from selection effects on D_n. To minimize them, we exclude all galaxies with σ below a fairly high cutoff. Most of the fits in Table 8 were made with log $\sigma_{cut} = 2.00$, but trials were also made using 2.20. As shown, there is little difference, and we adopt the value $D_n \sim \sigma^{1.20\pm0.1}$. The value of $x = 1.20$ adopted here differs slightly from the value 1.33 quoted by Dressler *et al.* (1987*b*). That value was intended to represent the "true" relation between D_n and σ, which is close to the mean of the regressions D_n on σ and vice versa. It is therefore larger.

The zero point in the relation is set by normalizing to Coma. All distances are expressed in km s^{-1}, bypassing the Hubble constant. In § VI we used the MC model to find an estimate for the peculiar velocity of Coma relative to the Hubble flow of −260 km s^{-1}. Coupled with the observed cluster velocity of 7200 km s^{-1} in the microwave rest frame, this implies that the unperturbed Hubble flow velocity at the distance of Coma is 7460 km s^{-1}. The median value of 1.2 log (σ) − log (D_n) in Coma for all galaxies with log (σ) ≥ 2.00 is 2.462, with D_n measured in 0.1. (This has been diameter-bias corrected; see below.) Applying the cosmology correction relative to Coma yields the raw distance estimator for field galaxies in equation (3.1). The raw value is then corrected by the Malmquist factor in equation (2.11). As different solutions have slightly different peculiar velocities for Coma, they have slightly different zero points.

In applying equation (3.1) to groups, there is another bias since most of the group samples are magnitude-limited and thus D_n-limited. Figure 10 shows that the group mean and median contain a contribution from too many large galaxies and too few small ones, and hence R is biased too small. Groups with large intrinsic scatter or just a few bright galaxies are affected the worst.

As noted by Schecter (1980), this second bias could have been avoided if we had determined the slope of the D_n-σ relation using the regression of σ on D_n rather than vice versa. However, such a fit would not follow the maxima of $p(D_n \mid \sigma)$ and hence would give biased distances for field galaxies compared to groups. It is clear that the shortcut approach of using a simple linear distance indicator for both field and group galaxies had led us into a dilemma—the optimum unbiased slope needed for groups is inherently different from that for field galaxies.

The proper way to deal with groups would be to determine group distances using $p(\sigma, d_n)$ and maximum-likelihood, but this would be time-consuming and complicated. Instead, we estimate how large the diameter-limited bias is and correct for it roughly. This was done by combining all galaxies with log $\sigma \geq 2.00$ in groups with more than three members using preliminary distances and cutting this sample at various levels of d_n. The response of the median distance indicator versus cut level (slightly smoothed) is given in Table 9.

The reader may ask why we need to worry about diameter-limited bias for clusters but not for single galaxies. This occurs for the following reason. The bias in the distance of any "object" is fully given by the Malmquist correction in equation (2.11), which applies equally well to single galaxies or clusters. This is not a magnitude-limited bias correction, as it applies to all objects independent of magnitude or any other selection limit. The separate diameter-bias correction for clusters enters when the cluster data are combined to create single "objects" out of several cluster members. Since this extra step does not occur for singles, no bias is introduced for them.

One might also ask why the cluster galaxies were combined to form normal points instead of being treated as separate data points like the single galaxies. The answer is the fact that the simple Malmquist distance correction is not applicable to cluster galaxies, as

TABLE 9

CORRECTIONS TO MEDIAN GROUP DISTANCES AS A FUNCTION OF D_n CUTOFF

log D_n(cut) + log (R)[a]	Δ log ($\sigma^{1.2}/D_n$)
3.76	0.000
3.81	0.002
3.91	0.005
4.01	0.009
4.11	0.017
4.21	0.028
4.31	0.041
4.41	0.055

[a] The units are 0.1 for D_n and km s^{-1} for R.

they are not distributed *a priori* uniformly in space. Once the cluster galaxies are grouped, however, it is plausible to assume that the clusters themselves are more or less uniformly distributed, and the simple Malmquist correction applies.

To summarize, distances to individual field galaxies are determined using equation (3.1) and corrected by the Malmquist correction in equation (2.11) using for Δ the value 0.21. For groups and clusters with more than one measured galaxy, a median value of l_e is computed (medians were preferred because of their greater stability against bad data). The median is corrected for the diameter-limiting bias using Table 9 and taking for d_n(cut) the diameter of the smallest galaxy observed in the group plus a preliminary distance based on the observed radial velocity (in Local Group coordinates). The Malmquist correction is then applied using equation (2.11), with Δ^2 replaced by Δ^2/N.

APPENDIX C

MAXIMUM-LIKELIHOOD METHODS

In this appendix we first derive an expression for the probability of observing an elliptical galaxy in our sample as a function of the observables D_n, v, and ln σ. We then show how to proceed with different versions of the maximum-likelihood method which make fewer assumptions.

Let d_n be the true ln (diameter) corresponding to the observed *angular* diameter D_n, and let $s = \ln \sigma$. Clearly,

$$d_n = \ln D_n + l \,, \tag{C1}$$

where $l = \ln r$ and D_n is in radians. Let $g(d_n, s)d\,d_n\,ds$ be the distribution of elliptical galaxies with ln (diameter) in the range d_n to $d_n + d\,d_n$ and ln σ in the range s to $s + ds$. In what follows we shall take g to be of the form that corresponds to expression (2.2) for l_e:

$$g = (2\pi\Delta^2)^{-1/2} n_1(s) \exp\left[-\tfrac{1}{2}(d_n - xs)^2/\Delta^2\right] , \tag{C2}$$

where $\int n_1(s)ds = 1$. If we rewrite d_n using equation (C1) and realize that $xs - \ln D_n$ is our estimated ln (distance), l_e, then it is clear that equation (C2) leads to equation (2.2). Again we take the number of elliptical galaxies in the cone of sight between l and $l + dl$ to be $n(l)dl$ as in equation (2.3). Then the distribution of ellipticals with radial velocities in v to $v + dv$, ln σ in s to $s + ds$, ln r in l to $l + dl$ and ln (angular diameter) in ln D_n to ln $D_n + d(\ln D_n)$ is $\varphi\,dl\,dv\,ds\,d(\ln D_n)$, where

$$\varphi(l, D_n, v, s) = n(l)g(\ln D_n + l, s)f(v \mid l) \,, \tag{C3}$$

where f is given by equation (2.6). We do not observe φ itself both because we do not know the true distances l and because we do not observe every elliptical galaxy. Thus there is a selection function $S(D_n, s)$ which gives the fraction of galaxies with given D_n and ln σ that are observed and accepted for analysis. From the discussion in § V*a*, S is zero for $s < \ln (100 \text{ km s}^{-1})$. In practice, there were few galaxies large enough to be in the sample but yet so dim as to prevent a σ determination so, S is primarily a function of D_n for the remaining range of s.

The probability "p" of observing a field galaxy in our sample with the values D_n, v, s is the suitably normalized integral of $S\varphi$ over all distances;

$$p(D_n, v, s) = S \int \varphi(l, D_n, v, s)dl/\Phi \,, \tag{C4}$$

where

$$\Phi = \iint S \iiint \varphi\,dl\,dv\,ds\,d(\ln D_n) \,. \tag{C5}$$

Writing out this expression in full using equations (C1), (C2), and (C3),

$$p = Sn_1(s) \int (2\pi\Delta^2)^{-1/2} n(l) \exp\left[-\tfrac{1}{2}(l - l_e)^2/\Delta^2\right] f\,dl/\Phi \,. \tag{C6}$$

The integral is precisely that evaluated in equation (2.7), and so, remembering expression (2.9) for F,

$$p(D_n, v, s) = \frac{Sn_1(s)n(l_e + \frac{1}{2}\alpha\Delta^2)}{\iint Sn_1 n\, ds\, d(\ln D_n)} F(v \mid R_e) . \tag{C7}$$

This is the expression for p that we needed. It consists of the distribution function F at the Malmquist-corrected distance R times a factor that we cannot estimate so reliably. We shall proceed with our description of the general method as though we knew p reliably and shall return later to variants of the method for which we only have to know F.

For each field galaxy i we calculate p_i by inserting into p the measured values of D_n, v, and σ and the observed direction of the galaxy $\hat{\boldsymbol{r}}$. We then form the giant probability P_1 of finding all the field galaxies as they are, $P_1 = \prod_i p_i$. The likelihood of the observed distribution on the basis of the assumed model is then

$$L_1 = \ln P_1 = \sum_i \ln p_i . \tag{C8}$$

L_1 will, of course, depend on all the parameters of the model, e.g., v_0, h, σ_e, Δ, x. The most likely model, given the data, is that which maximizes the likelihood with respect to all these parameters. The errors in this determination of parameters can be discovered by seeing how rapidly the likelihood falls as the parameters are varied away from the maximizing ones. This information is contained in the second derivatives of L_1 evaluated at the maximum.

Although the method just outlined may well be the best in principle, the answers it gives will depend on the mathematical forms chosen to represent the functions $n_1(s)$ and S. Although these forms may have several free parameters whose values are determined from maximizing L, nevertheless the parameters that characterize the best-fitting velocity field will depend on those mathematical forms.

It is possible to achieve answers without knowing all the functions involved in the above models by modifying the method to use conditional probabilities and the conditional likelihoods derived from them. We first illustrate what can be done by considering the case when, within the range considered, the selection function S is indeed a function of D_n alone. In place of the general probability $p(D_n, v, s)$ we consider the probability $p(v, s \mid D_n)$ of finding that a galaxy of given D_n has velocity v and a ln σ of s. Such conditional probabilities can be found from the formula

$$\begin{aligned} p(v, s \mid D_n) &= p(D_n, v, s) \Big/ \iint p(D_n, v, s) dv\, ds \\ &= n_1(s)n(\ln R)F(v \mid R_e) \Big/ \iint n_1(s)n(\ln R) ds , \end{aligned} \tag{C9}$$

where we have used equation (C7) and the assumption that S is a function of D_n alone. Notice that these conditional probabilities $p(v, s \mid D_n)$ do not involve the function S, so neither does the corresponding conditional likelihood L_2. We now ask under what circumstances does maximizing the conditional likelihood give the same unbiased answers for the parameters of the model as the true likelihood L_1. Since $p(v, s \mid D_n)$ is proportional to $p(D_n, v, s)$ it is clear that they will maximize the same parameter values provided the "constant" of proportionality is independent of the parameters maximized over. In the above case this means that we may maximize L_2 over all parameters except those involved in

$$\iint p(D_n, v, s) dv\, ds .$$

We would have to fix any parameters involved in that expression at their correct values by other considerations.

There is a greater weight of advantages in carrying this procedure a stage further. Consider the conditional probability $p(v \mid D_n, s)$ of finding that a galaxy of given D_n and s has radial velocity v. This can be found from the formula

$$\begin{aligned} p(v \mid D_n, s) &= p(D_n, v, s) \Big/ \int p(D_n, v, s) dv \\ &= F(v \mid R_e) , \end{aligned} \tag{C10}$$

where the last simplification arises by use of equation (C7). Notice that this result holds whatever the functions $S(D_n, s)$ and $n_1(s)$ may be. The corresponding conditional likelihood L_3 is the one that we use:

$$L_3 = \sum_i \ln F_i \tag{C11}$$

We may maximize L_3 over all the parameters not involved in $\int p(D_n, v, s) dv$. For those that are involved, maximizing of L_3 would give a biased result so they must be determined by another method. From equation (C7)

$$\int p(D_n, v, s) dv = \frac{S(D_n, s)n_1(s) \exp [\alpha(xs - \ln D_n)]}{\iint S(D_n, s)n_1(s) \exp [\alpha(xs - \ln D_n)] ds\, d \ln D_n} . \tag{C12}$$

Both top and bottom had a factor $\exp \frac{1}{2}\alpha^2\Delta^2$ which cancel, leaving the result independent of Δ^2. Expression (C12) clearly depends on x and α, but is independent of the parameters occurring in the model of the velocities. Thus the conditional likelihood has the advantages that neither S nor n_1 need be known and it gives unbiased answers when maximized over σ_f, Δ, and all the parameters

describing the velocity field. Its disadvantages are that α and x have to be determined from other considerations. We choose $\alpha = 3$ corresponding to the unbiased uniform distribution in the large, and we determine x from the slopes found in the well-observed clusters. We discuss the maximizing of L_3 in § V. Before doing that, we wish to point out how the velocity-width method can be viewed within our framework. Essentially, this method considers the question: Given a galaxy at angular diameter D_n and velocity v, what is the probability of it having a ln σ of s? The answer is

$$p(s \mid D_n, v) = p(D_n, v, s) \Big/ \int p(D_n, v, s) ds \, . \tag{C13}$$

The point of using the velocity-width method is to reduce Malmquist bias by reducing the dependence of the answer on the density distribution along the line of sight, $n(l)$. Any method of analyzing Hubble flow data must utilize some primary distance indicator. The velocity-width method uses measured radial velocity, v, in contrast to our method, L_3, which uses $\sigma^{1.2}/D_n$. As exemplified by equation (2.11), Malmquist errors enter owing to the fact that the distance estimates are not perfect. It is advantageous to use as accurate a distance indicator as possible, as Malmquist uncertainties are thereby minimized.

The attraction of the velocity-width method is that radial velocity is often a better distance indicator than $\sigma^{1.2}/D_n$ (or analogous indicators such as Tully-Fisher for spirals). This is especially true at large distances, where velocity noise, σ_f/v, is small. The crossover v is that distance where σ_f/v equals the fractional distance error of a single object. For the elliptical data, a typical normal point has an accuracy of order 15% and σ_f is 250 km s^{-1}, from which we infer that $v_{\rm cross} \approx 1700$ km s^{-1}.

Since most of our data lie beyond this distance, we could have minimized Malmquist uncertainties by using the velocity-width method. However, one pays a severe penalty for this—the function $\int p(D_n, v, s) ds$ depends on the parameters of the velocity field, so the likelihoods

$$L_4 = \sum_i \ln p_i(s \mid D_n, v) \tag{C14}$$

will maximize at biased values of the velocity field parameters. Since the nature of this bias is difficult to unravel, we have preferred the more straightforward method based on L_3, whose errors are easier to understand.[2]

APPENDIX D

THE GAUSSIAN APPROXIMATION TO THE VELOCITY DISTRIBUTION

Here we show that the distribution function $F(v \mid r_e)$ defined in equation (2.7) is well approximated by the Gaussian defined by equations (2.9)–(2.11). We do this by fitting the mean and standard deviation of F and then demonstrating that the third and fourth moments are so close to those of the Gaussian that our likelihoods are not significantly affected by the the Gaussian approximation.

The mean value of v in the distribution F is

$$\bar{v}(R_e) = \int v F(v \mid R_e) dv = (2\pi\sigma_f^2)^{-1/2} \iint v \exp - \left[\frac{1}{2} \frac{(v - He^l)^2}{\sigma_f^2} + \frac{1}{2} \frac{(l - l_e)^2}{\Delta^2} - \alpha(l - l_e) \right] dv \frac{dl}{I(\alpha)} \, , \tag{D1}$$

where

$$I(\alpha) = \int_{-\infty}^{\infty} \exp - [\tfrac{1}{2}(l - l_e)^2/\Delta^2 - \alpha(l - l_e)] dl = (2\pi\Delta^2)^{1/2} \exp (\tfrac{1}{2}\alpha^2 \Delta^2) \, . \tag{D2}$$

We shall need the formula

$$I(\alpha + n)/I(\alpha) = \exp \left[\Delta^2 n \left(\alpha + \frac{n}{2} \right) \right] . \tag{D3}$$

Now, if the double integral in equation (D1) had the initial v replaced by $v - He^l$, then the integrand would have been antisymmetric in $v - He^l$, so the integral would have been zero. Hence that first v may be replaced by He^l without changing the value of the integral. After performing trivially the resulting v integration we are left with an integral of the same form as I, but with $\alpha + 1$ replacing α. We thus obtain

$$\bar{v} = R_e I(\alpha + 1)/I(\alpha) = R_e \exp [\Delta^2(\alpha + \tfrac{1}{2})] = R \, .$$

The dispersion in v is obtained from

$$\sigma_e^2 = \int_{-\infty}^{\infty} (v - \bar{v})^2 F(v \mid R_e) dv = (2\pi\sigma_f^2)^{-1/2} \iint [(v - He^l) - (He^l - \bar{v})]^2 \exp - B \, dl \, dv / I(\alpha) \, ,$$

[2] One method used by AHMST is closely related to maximizing L_4. They explicitly noted the bias in the derived velocity field parameters noted above but did not mention the bias in the determination of the slope parameter, x. L_4, like L_3, gives a biased estimate of slope. The three other possible conditional probabilities,

$$p(D_n, v \mid s) \, , \quad p(D_n, s \mid v) \, , \quad \text{and} \quad p(D_n \mid s, v) \, ,$$

require a known selection function and the corresponding likelihoods are therefore less useful.

where B is the square bracket in equation (D1). Using the antisymmetry of the cross term in $v - He^l$, one readily obtains

$$\sigma_e^2 = \sigma_f^2 + R_e^2 \frac{I(\alpha+2)}{I(\alpha)} - \bar{v}^2 = \sigma_f^2 + R^2(\exp \Delta^2 - 1) .$$

We take the best-fitting Gaussian to be the one with the same $\bar{v}$ and σ_e^2 as in equation (2.10).

The third moment of v is given by

$$(2\pi\sigma_f^2)^{-1/2} \iint (v - \bar{v})^3 \exp - B\, dl\, dv/I(\alpha) .$$

The double integral is best evaluated by writing $(v - \bar{v})^3 = [(v - He^l) + (He^l - \bar{v})]^3$ and expanding the cube. The first three terms in such an expansion are zero, two of them by antisymmetry in $(v - He^l)$ and the third because the mean of He^l is $\bar{v}$. We are left with the average of $(He^l - \bar{v})^3$ which may be evaluated term by term to give

$$\langle (v - \bar{v})^3 \rangle = R_e^3 \left\{ \frac{I(\alpha+3)}{I(\alpha)} - 3\frac{I(\alpha+2)}{I(\alpha)}\frac{I(\alpha+1)}{I(\alpha)} + 2\left[\frac{I(\alpha+1)}{I(\alpha)}\right]^3 \right\}$$
$$= R_e^3 e^{3\Delta^2(\alpha+1/2)}(e^{3\Delta^2} - 3e^{\Delta^2} + 2) = R^3(e^{\Delta^2} + 2)(e^{\Delta^2} - 1)^2 .$$

The calculation of the fourth moment is similar

$$\langle (v - \bar{v})^4 \rangle = \langle [(v - He^l) + (He^l - v)]^4 \rangle = \langle (v - He^l)^4 \rangle + 6\langle (v - He^l)^2 (He^l - \bar{v})^2 \rangle + \langle (He^l - \bar{v})^4 \rangle$$
$$= 3\sigma_f^4 + 6\sigma_f^2 R^2(e^{\Delta^2} - 1) + R_e^4 \left\{ \frac{I(\alpha+4)}{I(\alpha)} - 4\frac{I(\alpha+3)}{I(\alpha)}\frac{I(\alpha+1)}{I(\alpha)} + 6\frac{I(\alpha+2)}{I(\alpha)}\left[\frac{I(\alpha+1)}{I(\alpha)}\right]^2 - 3\left[\frac{I(\alpha+1)}{I(\alpha)}\right]^4 \right\}$$
$$= 3\sigma_f^4 + 6\sigma_f^2 R^2(e^{\Delta^2} - 1) + R^4(e^{6\Delta^2} - 4e^{3\Delta^2} + 6e^{\Delta^2} - 3) .$$

The corresponding expression for the Gaussian with the same σ is

$$3\sigma_e^4 = 3\sigma_f^4 + 6\sigma_f^2 R^2(e^{\Delta^2} - 1) + 3R^4(e^{\Delta^2} - 1)^2 .$$

Hence for our non-Gaussian distribution

$$\langle (v - \bar{v})^4 \rangle = 3\sigma_e^4 + R^4(e^{\Delta^2} - 1)^3(e^{3\Delta^2} + 3e^{2\Delta^2} + 6e^{\Delta^2} + 6) .$$

The extra term makes a greater change in the fourth moment when σ_f is negligible, i.e., at large R. There the fractional change in the fourth moment (compared with the Gaussian approximation) is $(e^{\Delta^2} - 1)(\frac{1}{3}e^{3\Delta^2} + e^{2\Delta^2} + 2e^{\Delta^2} + 2)$ which is 0.25 for $\Delta = 0.21$. This corresponds to a 6% greater spread underlying the fourth moment for equal second moments.

A useful bound on our error in using the Gaussian approximation is obtained by imagining that in the wings of the distribution the probability is better given by fitting the fourth moments to a Gaussian instead of fitting the second moments. For a point 2 σ from the mean this would enhance the probability by $e^{0.11}$ and correspond to a likelihood increase of 0.11. To allow for the third moments, the wings need a shift of mean, but again the likelihood changes are only ± 0.1, the plus being on the side of increased velocity.

We deduce that changes from the Gaussian are small when the distance error is only 0.21 but the residuals should have somewhat larger wings than the Gaussian approximation and these should be slightly asymmetric.

REFERENCES

Aaronson, M., Bothun, G. D., Mould, J. R., Huchra, J., Schommer, R., and Cornell, M. 1986, *Ap. J.*, **302**, 536.
Aaronson, M., Huchra, J., Mould, J., Schechter, P. L., and Tully, R. B. 1982*a*, *Ap. J.*, **258**, 64.
Aaronson, M., Huchra, J., Mould, J., Tully, R. B., Fisher, J. R., van Woerden, H. H., Goss, W. M., Chameraux, P., Mebold, V., Siegman, B., Berriman, G., and Persson, S. E. 1982*b*, *Ap. J. Suppl.*, **50**, 241.
Bahcall, N. A., Soneira, R. M., and Burgett, W. S. 1986, *Ap. J.*, **311**, 15.
Bardeen, J. M., Bond, J. R., and Efstathiou, G. 1987, *Ap. J.*, **321**, 28.
Blumenthal, G. R., Faber, S. M., Primack, J., and Rees, M. J. 1984, *Nature*, **311**, 517.
Bond, J. R. 1987, in *Proc. Workshop on Nearly Normal Galaxies, From the Planck Time to the Present*, ed. S. M. Faber (New York: Springer-Verlag), p. 388.
Bond, J. R., and Efstathiou, G. 1984, *Ap. J. (Letters)*, **285**, L45.
Burstein, D., Davies, R. L., Dressler, A., Faber, S. M., Lynden-Bell, D., Terlevich, R. J., and Wegner, G. A. 1986, in *Galaxy Distances and Deviations from Hubble Expansion*, ed. B. Madore and R. B. Tully, (Boston: Reidel), p. 123.
Burstein, D., Davies, R. L., Dressler, A., Faber, S. M., Stone, R. P. S., Lynden-Bell, D., Terlevich, R. J., and Wegner, G. A. 1987, *Ap. J. Suppl.*, **64**, 601.
Burstein, D., and Heiles, C. 1984, *Ap. J. Suppl.*, **54**, 33.
Bushouse, H., Mellot, A. L., Centrella, J., and Gallagher, J. S., III. 1985, *M.N.R.A.S.*, **217**, 7P.
Chincarini, G., and Rood, H. J. 1979, *Ap. J.*, **230**, 648.
Collins, C. A., Joseph, R. D., and Robertson, N. A. 1986, *Nature*, **320**, 506.
da Costa, L. N., Nunes, M. A., Pellegrini, P. S., and Willmer, C. 1986, *A.J.*, **91**, 6.
Davies, R. L., Burstein, D., Dressler, A. J., Faber, S. M., Lynden-Bell, D., Terlevich, R. J., and Wegner, G. A. 1987, *Ap. J. Suppl.*, **64**, 581.
Davis, M., and Peebles, P. J. E. 1977, *Ap. J. Suppl.*, **34**, 425.
———. 1983, *Ap. J.*, **267**, 465.
de Vaucouleurs, G., de Vaucouleurs, A., and Corwin, H. G. 1976, *Second Reference Catalogue of Bright Galaxies* (Austin: University of Texas Press).
de Vaucouleurs, G., and Olson, D. 1982, *Ap. J.*, **256**, 346.
de Vaucouleurs, G., and Peters, W. L. 1981, *Ap. J.*, **248**, 395.
———. 1984, *Ap. J.*, **287**, 1.
———. 1985, *Ap. J.*, **297**, 27.
Dickens, R. J., Currie, M. J., and Lucey, J. R. 1986, *M.N.R.A.S.*, **220**, 679.
Djorgovski, S., and Davis, M. 1987, *Ap. J.*, **313**, 59.
Dressler, A., Faber, S. M., Burstein, D., Davies, R. L., Lynden-Bell, D., Terlevich, R. J., and Wegner, G. 1987*a*, *Ap. J. (Letters)*, **313**, L37.
Dressler, A., Lynden-Bell, D., Burstein, D., Davies, R. L., Faber, S. M., Terlevich, R., and Wegner, G. 1987*b*, *Ap. J.*, **313**, 42.
Faber, S. M., Burstein, D., Davies, R. L., Dressler, A., Lynden-Bell, D., Terlevich, R. J., and Wegner, G. 1987, in *Proc. Workshop on Nearly Normal Galaxies, From the Planck Time to the Present*, ed. S. M. Faber (New York: Springer-Verlag), p. 175.
———. 1988, in preparation.

Fall, S. M. 1975, *M.N.R.A.S.*, **172**, 23P.
Fixen, D. J., Cheng, E. S., and Wilkinson, D. T. 1983, *Phys. Rev. Letters*, **50**, 620.
Geller, M. J., and Huchra, J. P. 1983, *Ap. J. Suppl.*, **52**, 61.
Harmon, R. T., Lahav, O., and Meurs, E. J. A. 1987, *M.N.R.A.S.*, **228**, 5P.
Hart, L., and Davies, R. D. 1982, *Nature*, **297**, 191.
Haynes, M. P., and Giovanelli, R. 1986, in *Galaxy Distances and Deviations from Universal Expansion*, ed. B. Madore and R. B. Tully (Boston: Reidel), p. 117.
Hopp, U., and Materne, J. 1985, *Astr. Ap. Suppl.*, **61**, 93.
Huchra, J. P., and Geller, M. J. 1982, *Ap. J.*, **257**, 423.
Humason, M. L., Mayall, N. U., and Sandage, A. R. 1956, *A.J.*, **61**, 97.
Lahav, O. 1987, *M.N.R.A.S.*, **225**, 213.
Lahav, O., Rowan-Robinson, M., and Lynden-Bell, D. 1988, *M.N.R.A.S.*, in press.
Lauberts, A. 1982, *ESO/Uppsala Survey of the ESO(B) Atlas* (Garching: ESO).
Layzer, D. 1963, *Ap. J.*, **138**, 174.
Lilje, P., Yahil, A., and Jones, B. J. T. 1986, *Ap. J.*, **307**, 91.
Lubin, P. M., Villela, T., Epstein, G. L., and Smoot, G. F. 1985, *Ap. J. (Letters)*, **298**, L1.
Lucey, J. R. 1986, *M.N.R.A.S.*, **222**, 417.
Lucey, J. R., Currie, M. J., and Dickens, R. J. 1986, *M.N.R.A.S.*, **221**, 453.
Lynden-Bell, D. 1986, *Quart. J.R.A.S.*, **27**, 319.
———. 1987, *Quart. J.R.A.S.*, **28**, 186.
Meiksin, A., and Davis, M. 1986, *A.J.*, **91**, 191.
Melnick, J., and Moles, M. 1987, *Proc. 5th IAU Regional Meeting* (Mexico).
Nilson, P. 1973, *Uppsala General Catalogue of Galaxies* (*Uppsala Astr. Obs. Ann.*, Vol. **6**).
Peebles, P. J. E. 1971, *Physical Cosmology* (Princeton: Princeton University Press).
———. 1980, *The Large Scale Structure of the Universe* (Princeton: Princeton University Press).
Peterson, C. J., and Baumgart, C. W. 1986, *A.J.*, **91**, 530.
Rubin, V. C., Ford, W. K., and Rubin, J. S. 1973, *Ap. J. (Letters)*, **183**, L111.
Rubin, V. C., Ford, W. K., Thonnard, N., Roberts, M. S., and Graham, J. A. 1976*b*, *A.J.*, **81**, 687.
Rubin, V. C., Thonnard, N., Ford, W. K., and Roberts, M. S. 1976*a*, *A.J.*, **81**, 719.
Schechter, P. L. 1980, *A.J.*, **85**, 801.
Shaya, E. J. 1984, *Ap. J.*, **280**, 470.
Staveley-Smith, L. 1985, Ph.D. thesis, University of Manchester.
Tammann, G. A., and Sandage, A. 1985, *Ap. J.*, **294**, 81.
Terlevich, R. J., Davies, R. L., Faber, S. M., and Burstein, D. 1981, *M.N.R.A.S.*, **196**, 381.
Tully, R. B., and Shaya, E. J. 1984, *Ap. J.*, **281**, 31.
Villumsen, J. V., and Davis, M. 1986, *Ap. J.*, **308**, 499.
Vittorio, M., Juszkiewicz, R., and Davis, M. 1986, preprint.
Vorontsov-Velyaminov, B., and Archipova, V. 1963, *Morphological Catalogue of Galaxies, Parts III and IV* (Moscow: Moscow University Press).
Weinberg, S. 1972, *Gravitation and Cosmology* (New York: J. Wiley).
White, S. D. M., Frenk, C. S., Davis, M., and Efstathiou, G. 1987, *Ap. J.*, **313**, 505.
Yahil, A., Walker, D., and Rowan Robinson, M. 1986, *Ap. J. (Letters)*, **301**, L1.

DAVID BURSTEIN: Physics Department, Arizona State University, Tempe, AZ 85281

ROGER L. DAVIES: KPNO, National Optical Astronomy Observatories, P.O. Box 26732, Tucson, AZ 85726-6732

ALAN DRESSLER: Mount Wilson and Las Campanas Observatories, 813 Santa Barbara Street, Pasadena, CA 91101-1292

SANDRA FABER: Lick Observatory, University of California, Santa Cruz, CA 95064

DONALD LYNDEN-BELL: Institute of Astronomy, The Observatories, Madingley Road, Cambridge CB3 0HA, England

ROBERTO TERLEVICH: Royal Greenwich Observatory, Herstmonceux Castle, Hailsham, East Sussex BN27 1RP, England

GARY WEGNER: Department of Physics and Astronomy, Dartmouth College, Wilder Laboratory, Hanover, NH 03755